ANALYSIS AND OPTIMIZATION OF ELECTROFORMED DENDRITIC STRUCTURES AS ENHANCED HEAT TRANSFER SURFACES

A Thesis presented to the Faculty of the Graduate School
University of Missouri

In Partial Fulfillment
Of the Requirements of the Degree

Master of Science

---

by
MICHAEL CAMPBELL

Dr. Hongbin Ma, Thesis Advisor

MAY 2009

The undersigned, appointed by the Dean of the Graduate School, have examined the thesis entitled:

ANALYSIS AND OPTIMIZATION OF ELECTROFORMED DENDRITIC STRUCTURES AS ENHANCED HEAT TRANSFER SURFACES

Presented by Michael Campbell

A candidate for the degree of Master of Science, and hereby certify that, in their opinion, it is worthy of acceptance.

_____

Professor Hongbin Ma

_____

Professor Gary Solbrekken

_____

Professor Bin Wu

To my wife Amy,
who, despite all evidence to the contrary, still believes I am infallible.

SPECIAL THANKS:

Dr. Hongbin Ma
Dr. Gary Solbrekken
Dr. James Bryan
Corey Wilson

Table of Contents

List of Figures

List of Tables

Nomenclature

A	Acidity
C	Current Density
CA	Current/Acid Interaction
CAS	Total Interaction
E	Main Effect
H_a	Alternative Hypothesis
H_0	Null Hypothesis
k	Number of parameters in a factorial analysis
n	Total number of test conditions
N	Total number of test conditions, including replications
S	Salt concentration
s^2	Variance of repeated test conditions
SA	Salt/Acid Interaction
SC	Salt/Current Interaction
s^2_{effect}	Sample variance of effects
s^2_p	Pooled variance
t	Student-t value

Greek

μ_{effect}	Mean value of effect

Abstract

Over the past several years, the use of passive cooling devices in electronics such as heat pipes and vapor chambers has increased. Due to their more widespread use, these technologies have a high demand for more adaptable manufacturing and increased efficiency. The choice in wicking structure in these devices has been limited to trading efficiency for manufacturability or vice versa. Using an electroforming process, a new wicking structure has been designed which can optimize the balance between these two extremes. This new process forms a wick which can be grown on virtually any metal surface and on almost any geometry. In addition, the effective thermal conductivity, capillary pumping power, and permeability of this wick can be controlled during its manufacture by varying the electroforming process's parameters. By changing the acidity, salt content, and current density of the electroforming bath, a wick can be generated to meet the requirement of high heat flux applications.

Chapter 1: Wicking Structures

MOTIVATION and HISTORY

A major limiting factor for future electronic devices will be the excess heat they produce. These devices are decreasing in size and their power requirements are increasing, thus leading to much higher and much more concentrated heat flows. There are numerous cooling devices which have been developed to remove this excess heat. Of the numerous systems designed to transport heat, the heat pipe and vapor chamber are among the most efficient. The advantage to using this technology is that large heat fluxes can be transported from small surface areas to larger, more manageable, surface areas.

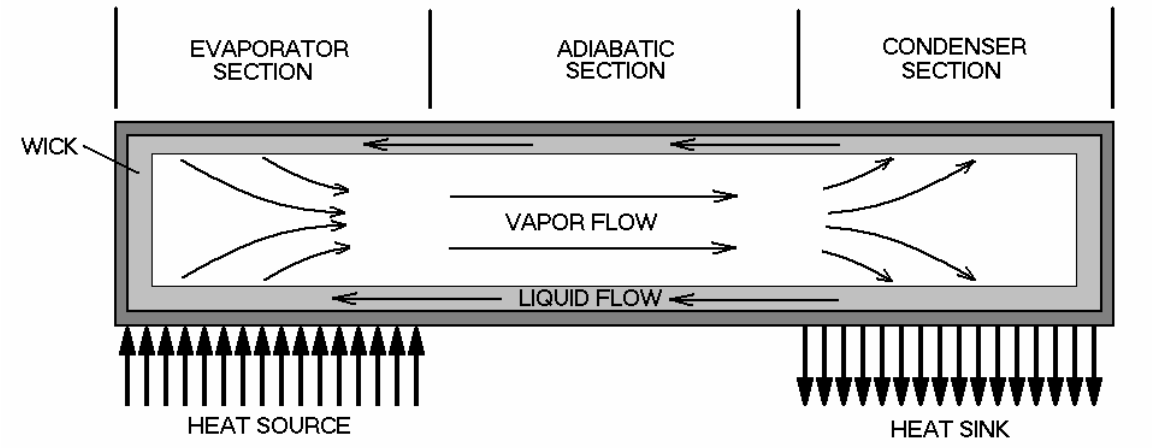

Figure 1. Schematic of a conventional heat pipe

The operation of a heat pipe is simple, but offers many variations. The simplest version of the heat pipe, the cylinder, can be seen in Figure 1. The main components of a heat pipe are a wick structure and a working fluid that exists in equilibrium with its vapor phase. The heat pipe has three parts: evaporator, adiabatic or transport, and condenser sections. Heat is applied to the evaporator

section of the heat pipe and this vaporizes the working fluid in that section. The expansion of this vapor causes a “vapor pressure”, which drives the vapor through the adiabatic section to the condenser. Here, the vapor condenses and releases its latent heat into the heat sink. The resulting condensed liquid uses the capillary pressure from the wick to travel back to the evaporator section and the process repeats. This device allows for the continuous transportation of heat.

> The introduction of the heat pipe was first conceived by Gaugler (1944) of the General Motors Corporation in the U.S. Patent No. 2350348. [1] Gaugler, who was working on refrigeration problems at that time, envisioned a device which would evaporate a liquid at a point above the place where condensation would occur without requiring any additional work to move the liquid to the higher elevation. His device consisted of a closed tube in which the liquid would absorb heat at one location causing the liquid to evaporate. The vapor would then travel down the length of the tube where it would recondense and release its latent heat. It would then travel back up the tube by capillary pressure to start the process over. [2]

Gaugler envisioned using a sintered iron wick as a device for moving the fluid to a higher point. Although General Motors rejected the idea, the idea of using this technology eventually took hold with the space program. The first recognition of the heat pipe as a viable device would have to wait until 1965 when a theoretical analysis suggested the reliability of this device was feasible.

The wick structure within a heat pipe or vapor chamber exists to return the condensed working fluid back to the evaporator section. There are dozens of different types of wick structures, all designed in an attempt to optimize the performance of the heat pipe. There are two main types of wicks: homogeneous and composite. The focus here will be on homogenous wicks due to their

simplicity in design, manufacturability and installation. Homogeneous wicks are characterized by their use of one material or one fabrication technique. The most common of these are the screen wick (a metal or cloth fabric) and the sintered metal wick (tightly packed metal particles). There are three main properties of wicks which are of the most importance in heat pipe design:

1. Minimum capillary radius
2. Permeability
3. Effective thermal Conductivity

The minimum capillary radius should be kept as small as possible to allow for higher pumping pressures. Minimum capillary radius is important when considering cases where high heat transport is required. The permeability of a wick refers to the wick's resistance to liquid flow. This parameter should be as small as possible to reduce the liquid pressure drop. The effective thermal conductivity is the wick's ability to transport heat through a porous medium. It is essential to keep this value high for a small temperature drop across the wick. It would be impossible to maximize these three without negatively affecting the other two. For example, a large effective thermal conductivity would result from having a small minimum capillary radius, but the permeability would suffer greatly. When designing a wick, it is important to determine which parameters are most important to the case at hand. In cases where a high heat transport is needed, it would be best to minimize the minimum capillary radius. In cases where fluid transport is paramount, optimizing the wick's permeability would be best. In short, it would be in the designer's best interest to have a homogenous

wick which can be modified during its fabrication to optimize the parameter which best fits the application.

The two main parameters of a wick which drives these three properties is porosity and pore radius. For example, a sintered powder wick would be good in a situation where high effective thermal conductivity and high capillary pressure were needed, but it has very low permeability. This is due to the high ratio of metal to voided areas in the wick. The porosity and pore radii are both low. Another good example of a wick is an axial groove wick (commonly used in heat pipes). This wick, depending on the groove type (triangular, rectangular, trapezoidal, etc...), can eliminate the issues associated with low effective thermal conductivity. Since the grooves are large compared to the pores of a sintered metal powder, the permeability is quite high comparatively. However, since the wetted perimeter of the grooves is low due to high "pore" size, the pumping ability is quite low and can have significant problems in gravity-sensitive applications. Sintered metal powder and axial grooves have very distinctive vertical porosity profiles which can be seen in Figure 2.

Vertical porosity profiles can describe a large amount about the final wick effectiveness. By forming an interfacial shape that has a changing radius, like a dendritic wick, one can establish a pressure gradient in the liquid film, which drains condensate from the surface. [3] The profile for sintered powder wicks found in Figure 4 describes a wick which is very porous at the top and bottom of the wick, but very solid in the middle. This type of profile would be very good in situations where vapor entrainment would be an issue. The higher porosity of the

wick near the base allows for preferential liquid flow paths ideal for the transport (adiabatic) section of heat pipes.

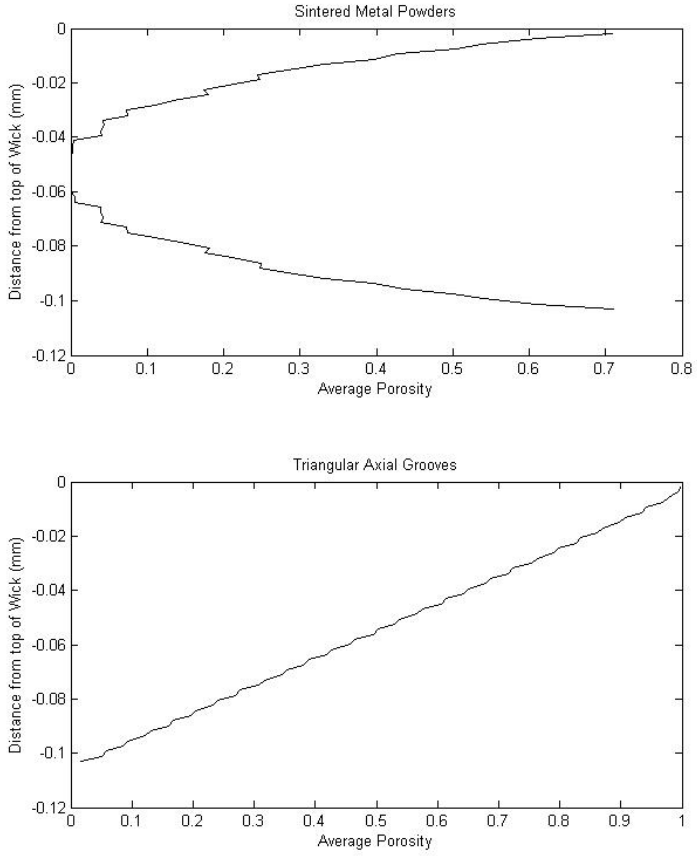

Figure 2. Porosity profile for sintered powder wicks and axial groove wicks

Both of the examples above are good examples of wicks for a certain application. However, both wicks have significantly different manufacturing processes and would require two vastly different sets of equipment to manufacture. If the porosity and pore radius of a wick can be precisely controlled during fabrication, it would make great strides in optimizing heat pipe manufacturing and optimization.

In the current investigation, an electroforming method for fabricating wicks is developed. This procedure (described in the following sections) utilizes an electrodeposition method which can be used to create dendritic copper wicks with controllable porosity and pore size. With this innovative method, the procedure can be modified to yield a dendritic wick which has a desired porosity, minimum meniscus radius, and thermal conductivity that best fits the application.

The dendritic ("tree-like") phenomenon is seen in nature with great frequency. "The tree design is robust with respect to various modifications in its internal structure. This means that the global performance of the system is relatively insensitive to changes in some of the internal geometric details. Trees that are identical have nearly identical performance." [4] The idea of a large surface area with many geometric extremes but with a common unifying base point is very important in heat transfer. To be able to use this natural optimization of aspect ratio to create effective heat and fluid flow paths is a significant motivation for this investigation.

Chapter 2: Electroforming/Electroplating

Electroplating is the process that uses electrical current to coat an electrically conductive object with a thin layer of a material, usually a metal. While copper electrodeposition processes were originally done in 1810 and a technical report was published in 1836, most electrodeposition work was done in the mid-1900's, so most information on these processes come from this era. Any further discussion on electroplating in general will be referring specifically to the Acid Copper Sulfate electrodeposition process. Electroplating has two major components: a fluid known as an electrolyte and an electrical system consisting of an anode and cathode as shown in Figure 3. The electrolyte consists of sulfuric acid, water and a salt called cupric sulfate. Hydrochloric acid and "brighteners" are often used to decrease the electrical resistance of the bath and refine the grain size of the final product, respectively. These are not included in this thesis due to their adverse effects in creating dendritic copper wicks. The part being plated, sometimes called the substrate, is the cathode of the circuit. In Acid-Copper plating, the source of the ions is known as the anode. Both of these parts are immersed in the electrolyte and an electrical current is applied between them.

A simplified example of how electroplating works is given in Lowenheim [5]. The first step is both the cathode and anode are immersed into the electrolyte. In this example, cupric sulfate is generally considered to be completely ionized, so only copper and sulfate ions are found in the bath. With a power supply, electrons are supplied to the cathode. A copper ion in the bath, being positively charged, is attracted to the cathode, which has an excess of

electrons. This copper ion from the bath now consumes the electrons on the surface of the cathode and becomes an atom, attaching (discharging) to the cathode. In response, an atom at the anode releases two electrons and becomes a positively charged ion in the bath. This process repeats billions of times and will eventually plate a small layer of copper on the substrate.

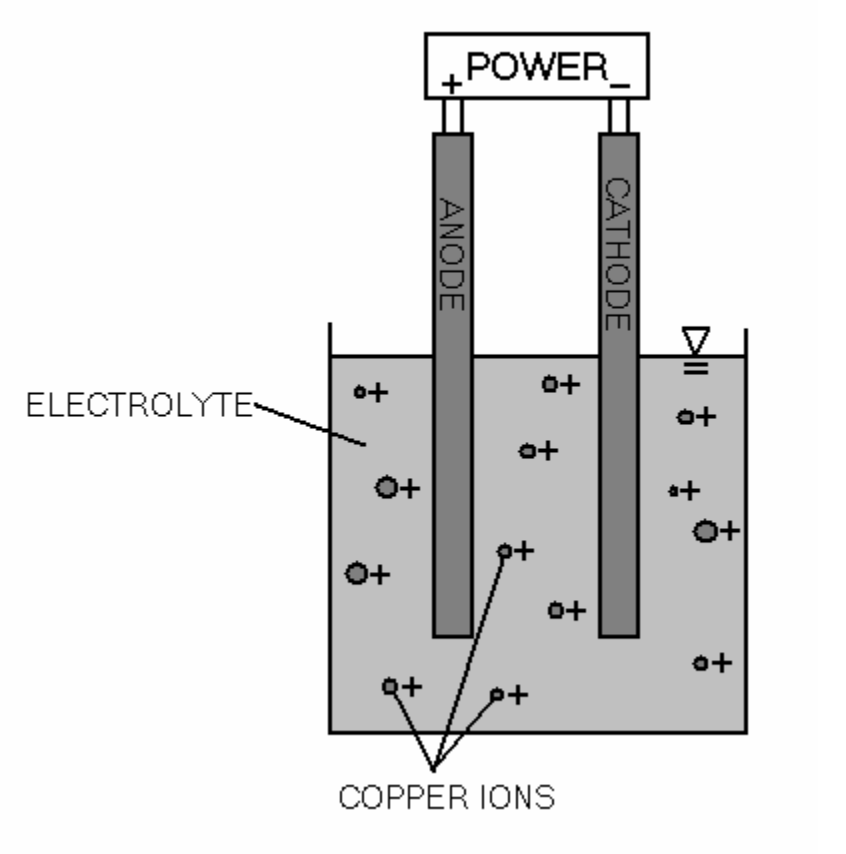

Figure 3. Simplified schematic of an electroplating bath

Materials Science Background

Just like most metals, copper has a crystalline structure. Copper's structure is described as a face-centered cubic (FCC). In electrodeposition processes, a crystallite is a small group of unit cells which are usually disoriented with respect to its neighbors. Electrodeposits take on this form in the bath. In

other words, the structure of a crystallite is usually several smaller “chunks” of randomly oriented grains. Electrodeposits develop initially as discrete particles, but upon joining, may form one crystal. [6]

In any metal, there are defects. This can take on the form of spot defects, such as metal impurities or vacancies in the lattice, or planar defects such as grain boundaries. There is a special type of boundary which is common in electrodeposits called a “twin.” Twins are volumes of material bounded by two parallel planes. The crystal lattice in the “twin” is the mirror of that on the other side of the twinning plane.

In plating operations, the surface properties of the substrate, as well as the deposit, are of practical importance. Surfaces are very different from the interior because the atoms have fewer neighbors and are therefore more unstable and have a higher energy. This surface energy is created when a surface is formed by propagating a dislocation. Due to this higher inherent energy, the surface will take on foreign atoms to take the place of the “missing” metal atoms. Adsorption occurs when gas molecules take the place of these atoms on a surface. This occurs preferentially at sites of surface irregularities. Adhesion strength depends on the condition of the surface. If the surface is free of oxides and other foreign materials, the atoms of the deposit can assume the positions of the missing neighbors. This metallic bond that is formed when the surface is free of impurities is very strong. This is opposed by the bonding to oxides, which is very weak. Because of copper’s affinity for oxygen bonding, it is important for the cathode substrate to be free of oxidation.

Electrodeposit Structures

When a metal is deposited, it will try, if possible, to match the structure of the substrate. When definite crystal planes and are parallel in the deposit and the substrate, this is called epitaxy. In electrodeposition processes, epitaxy is desired because there is better metallic bonding when epitaxy occurs. In this case, a copper/copper deposition process is very good because the substrate and deposit have the same structure and lattice parameter. For example, if a {1 0 0} plane is parallel to the surface, the same crystal plane of the deposit is parallel to the surface. The first atom layers of an epitaxial deposit are stretched or compressed to the same interatomic spacing as the substrate (This deposit is said to be pseudomorphic). As the thickness of a deposit grows, the interatomic spacing "fixes" itself and will eventually be uniform and be free of pseudomorphic stresses.

Kink sites are suitable sites for epitaxial deposition, usually at the end of incomplete atoms. The electrodeposit is discharged on the substrate and diffused at one of these kink sites. The alternative is for the deposit to diffuse into the solution and stay there until it approaches a kink site and discharges. Foreign species in electroplating and electroforming such as addition agents and chemical impurities can (either intentionally or unintentionally) be absorbed at these kink sites and prevent the spreading of the monolayer (an atom thick layer on the substrate). Then, subsequent layers are prevented from forming around this kink site. This phenomenon is called "bunching." In general, the more impurities in the bath, the smaller the lateral dimensions of the three-dimensional structures formed from bunching.

In actual plating processes, epitaxial deposition does not occur perfectly on the entire monolayer, but usually in the formation of small, three-dimensional "crystallites," as discussed before. These crystallites coalesce to form a group. This is why electroplated materials contain large amounts of dislocations.

In plating solutions with a low concentration of foreign substances, (eg. Cu with no "brightening" or addition agent) epitaxial growth continues throughout the thickness. This produces grains with a columnar shape. In plating solutions with a high concentration of foreign substances, epitaxial growth is limited to very thin deposits. All layers which constitute a single "grain" are epitaxial because each layer is the substrate for the subsequent layer. This next layer must have the same crystal plane parallel to the current layer. The thickness of the epitaxial deposit layer depends on the composition of the plating solution and grain orientation. This thickness is greater in copper acid plating when the {1 0 0} plane is parallel to the surface.

If the substrate's surface is such that an epitaxial growth is impossible (the number of kink sites is very limited), new grains must be nucleated. This condition occurs when a foreign deposit blocks kink sites or if atoms arrive in large numbers. This is the case when the current density of the electroforming process is proportionally large to the substrate surface area. New grains are likely nucleated by atoms meeting to form three dimensional arrays consisting of a few unit cells. When these new grains are nucleated, grains with certain crystal planes ({1 0 0}) parallel to the surface grow faster in the direction perpendicular to the substrate's surface. These faster growing grains also spread laterally until they meet other grains of the same orientation. Grains with other orientations become

covered and cease to grow. This leads to certain deposit orientations (grown planes which are parallel to the deposit) to grow preferentially.

The fiber texture that results from this phenomenon depends on plating solution composition, deposition potential (current density), and bath agitation. Certain additives can alter the fiber axis or cause the deposit to become randomly oriented. Brighteners result in fine grains and limit the perpendicular growth that is desired in dendritic copper structures that make up a wick, so they are omitted in the bath. High current density generally results in fine grains, but very low current densities can also produce small grains due to the long length of time before metal atoms are incorporated at kink sites. High current densities result in grain refinement but promote the growth of “nodules and trees.” [6] This favors their being blocked by brighteners. Recall that when kink sites are blocked, new grains must be nucleated. High solution temperatures encourage metal atom incorporation at kink sites, leading to large grains. An increase in acid concentration (higher Ph) at the substrate surface results in the formation of growth inhibiting substances, which results in smaller grain size.

So, bath constituents play a large role in the final microstructure and macrostructure of the plated copper and the three main components to obtain a certain desired final surface condition are sulfuric acid concentration, cupric sulfate concentration and current density.

Electroforming Procedure

BATH SETUP

The bath's constituents are the most essential part of obtaining a viable copper wick. Cupric Sulfate and Sulfuric Acid concentrations are the key to this procedure. These steps should be executed with care.

1. Obtain a vessel for containing the bath. This vessel should have the following characteristics:
    a. It should be plastic or glass. Beakers work great for small sample applications.
    b. There should be some method of agitation. For example, a stirring hotplate for small sample applications is best.
2. Fill the vessel with a known volume of distilled water. Tap water is unacceptable because of the large amounts of impurities.
3. Using a high-precision scale, measure out the desired amount of Sulfuric Acid. The amount of this acid needed will vary depending on the wick type desired, so read the results section on concentration levels for more information.
4. Start the agitation of the bath.
5. Very slowly, decant the acid into the water. Take your time. The Sulfuric Acid distillation reaction is very exothermic and if taken too quickly, will cause evaporation of the acid. Never add water to the acid, this will sometimes cause rapid evaporation or boiling and is very dangerous.
6. Using a high-precision scale, measure out the desired amount of Cupric Sulfate. The amount of this salt needed will vary depending on the wick

type desired, so read the results section on concentration levels for more information.

7. Slowly add the cupric sulfate to the bath and allow all of the powder to dissolve completely into the fluid.
8. For best results, allow this solution to sit undisturbed for a few minutes until the temperature falls back down to ambient. If it is a particularly acidic solution, this may take a few hours and a short bath in cold water can be used.

SURFACE PREPARATION

The surface on which the dendritic copper will be grown should have all foreign impurities (oxidation, dirt, etc.) removed with a scouring pad or similar device. This section describes one way of achieving a desirable substrate surface. All of these steps should be done with gloves as acetone and DuraClean can cause skin irritation.

1. To ensure even bonding to the substrate, the surface must be relatively flat and even. This can be achieved by pressing the sample between two steel blocks in a vice.
2. The substrate will need to have some source of electricity when the process starts. A copper wire fed through a hole in the substrate works fine. Make sure there is good electrical contact between the cathode wire and substrate.
3. The surface on which the dendritic structure will be formed should first have all superficial matter removed from it. This is easily done with a scouring pad or sandpaper.

4. When the surface has been polished as well as possible, use a “squirt bottle” filled with acetone and spray down the sample. This step removes any accumulated oils and greases that may have been applied by human hands. It also removes any small grit left behind by the polishing process.
5. DuraClean can be used here as a device for removing oxidation from the surface. However, it should be noted that if the DuraClean is allowed to evaporate from the surface, there is a good chance that surface will oxidize quickly. Only use DuraClean if the surface is particularly greasy or oily.
6. Use a paper towel (not cotton) to remove the acetone from the surface. From here on, it is best to avoid all direct contact with the target surface.

At this point, the substrate should be flat, clean and have an electrical wire attached somewhere to it. The bath should be well mixed and down to room temperature.

WAX APPLICATION

There are several methods for ensuring that the dendritic structure grows only on desired surfaces. The most effective of these is the wax-removal method. Beta wax, or jeweler’s wax has a strong resistance to acetone and sulfuric acid.

1. The wax should be melted in a ceramic dish. A double boiler setup is preferred. If time is an issue, short bursts from a propane torch can be used to speed the melting process. Constant high heat fluxes on the wax cause it to vaporize. “Low and slow” is a better method.
2. Careful forward planning will ensure that this procedure is not messy:
    a. Have a “receiving” dish ready to catch the wax runoff.

b. This is best done with two people. One person pours the wax, the other holds and rotates the substrate.
c. Heat resistant gloves should be worn by both parties.

3. Using pliers, firmly grasp the ceramic dish with the melted wax.
4. Position the substrate above the “receiving” dish.
5. Pour wax over the areas of the substrate upon which the dendritic wick will NOT be applied. This does not need to be extremely accurate, as the wax can be removed with a razor blade after cooling.
6. Allow the wax to cool for at least two minutes or until the wax no longer holds a thumbprint.
7. Remove excess wax in areas where the dendritic structure will be applied using a razor blade.

ANODE PREPARATION

The anode is a very important part of the electroplating process. While the geometry of the anode is not especially crucial, shapes with areas of high potential (sharp edges and corners) should be avoided. An anode with considerable bulk is desired for multiuse applications.

1. To the anode, firmly attach with solder or vinyl tape a wire that can be fed into the power supply. Solder works best in this situation for good electrical contact.
2. Lower the anode carefully into the bath until an appropriate amount of surface area is exposed to the electrolyte. The amount of surface area exposed will vary depending on the wick type desired, so read the results section on concentration levels for more information.

3. Connect the wired end of the anode to the positive side of an appropriate direct current (DC) power supply.

FORMING

1. Lower the cathode carefully into the bath and attach the wired end to the negative side of a DC power supply.
2. Make sure both the anode and cathode are secure enough to withstand a small amount of fluid flow and that they are not touching.
3. Turn on the agitation of the bath (pump or stirring hotplate).
4. Turn on the power supply to the appropriate current density. The current density will vary depending on the wick type desired, so read the results section on concentration levels for more information.
5. Let the system run for the appropriate amount of time. The amount of time will vary depending on the wick type and thickness desired, so read the results section on concentration levels for more information.

Chapter 3: Electroforming Dendritic Wicks

While the concept of acid-copper electroplating is an old one, the concept of electroforming dendritic copper wicks is a relatively new one. The idea of using electroforming and electroplating processes to create porous structures for heat transfer enhancement is fairly common. For example, Fujii [7] used electroplating to bond several layers of fine copper particles to the base surface and Shum [8] formed a porous coating by integrating graphite particles into the electrolyte. However, the idea of using an unmolested electrolyte to grow a wick directly onto an otherwise unaltered surface is unique. This concept started in 2008 as an accident when a former researcher, Chris Vincent, was attempting to electroform preset shapes for Oscillating Heat Pipe channels. [9] By coincidence, the parameters of the setup were ideal for forming a dendritic copper structure and the first “fuzzy copper” wick was created. While the exact reason for this original iteration is a mystery, the proof of concept was there and the need for investigation was apparent.

While this “fuzzy” phenomenon is not new, nearly all of the electroplating and electroforming researchers found it to be an undesirable deviation from their goals. Therefore, there has been very little (if any at all) exploration into the exact cause. A literary review shows that most researchers give vague parameterizations of the cause of these structures (eg. “low acid”, “high current density”, “low brightener”). Numerous papers have been written and several patents filed using electroforming as a way to create porous copper for evaporation and condensation. [10, 11, 12] However, in each of those cases, the

electrodeposition phenomena was observed, but not investigated. It became apparent that more research needed to be done with the optimization of fluid flow and heat transfer in mind.

After a few months of failed attempts to theoretically explain the exact parameters needed to replicate these “fuzzy” copper results, a more systematic approach was taken. Several superficial tests were run to narrow the ranges of acid, salt and current concentrations to values which consistently resulted in the formation of dendritic structures. The next step was to design an experiment which would narrow down the array of parameters into one or two that affect the final porosity of the wicking structure the most.

STATISTICAL DESIGN - 2^k FACTORIAL EXPERIMENT

The ability of an experimental design to observe the effects of changing factors individually with all other factors held constant is important. However, when there are multiple parameters that may affect the final outcome, this can become immensely time consuming and prohibitively expensive. For example, in this case, there are three parameters which may affect the final product: current density applied to the system (C), acid concentration in the solution (A), and cupric sulfate concentration in the solution (S). If one were to take just ten points along a range of each of the parameters, it would involve running $10^3 = 1{,}000$ tests. This is not acceptable in a lab environment, nor is it practically necessary to obtain verifiable results. Instead, a factorial experiment can be run on the three parameters which tests the upper and lower bounds of each of the parameters and observes which parameters are statistically significant. This process is laid out in DeVor [13] and modified to fit the experiment at hand. A complete factorial

design with three parameters contains eight unique test conditions. These test conditions are given in Table 1.

Table 1. Test conditions

	C	A	S
1	-	-	-
2	+	-	-
3	-	+	-
4	+	+	-
5	-	-	+
6	+	-	+
7	-	+	+
8	+	+	+

In Table 1, the pluses (+) are considered the upper bound of that particular parameter and the minuses (-) are considered the lower bound of that parameter. The target values for the tests (described in more depth later) this chart can be seen in Table 2.

Table 2. Test conditions with values

	C	A	S
1	0.4 A	2.9 g/L	15 g/L
2	1.5 A	2.9 g/L	15 g/L
3	0.4 A	20 g/L	15 g/L
4	1.5 A	20 g/L	15 g/L
5	0.4 A	2.9 g/L	30 g/L
6	1.5 A	2.9 g/L	30 g/L
7	0.4 A	20 g/L	30 g/L
8	1.5 A	20 g/L	30 g/L

The final effect will be a measurement of the porosity of the final dendritic structure as it relates to the industry “desirable effect” which is to plate smooth (a porosity of zero) However, any quantifiable final effect and derivations thereof (effective thermal conductivity, permeability, effective pore radius) can be calculated using this method.

To judge the relative importance of a variable effect based on calculated main and interaction effects, replicated tests are used to estimate the error

expected. The first step is to calculate the pooled variance, which is given by the expression

$$s_p^2 = \frac{\sum s^2}{n} \qquad (1)$$

where s^2 is the variance of the repeated test condition and n is the number of total test conditions. Next, it is necessary to find the main effect (E) of each of the four variables and the effect of any interaction effects. The main effect is defined as the average of the differences (or contrasts) between two opposing test conditions. For example, the calculation of one main effect value would be two tests which have opposing values of acid content (high and low) but are otherwise identical. The main effect is more precisely calculated by following these steps:

1. Find the average porosity of the replicated runs for each test number. For example, if there is one replication, take the average of the two for each test number.
2. Sum up the upper bound averages for each variable. For example, for the salt concentration variable (S), you would sum up the results of tests 5 through 8.
3. Sum up the lower bound averages for each variable. For example, for the salt concentration variable (S), you would sum up the results of tests 1 through 4.
4. Subtract the lower bound value found in step 3 from the upper bound value found in step 2.
5. Divide this number by the total number of tests (8 in this case)

Repeat these steps for each of the variables. Also remember to do this for all interaction effects. Interaction effects are the "multiplication" of two or three variables. For the results of these calculations, see the results section.

Using the pooled variance result, the sample variance of the effects can be calculated using the expression

$$s_{effect}^2 = \frac{4s_p^2}{N} \tag{2}$$

where N is the is total number of tests conducted, including replications. For example, if the eight tests were replicated once, N would be 16. With this sample effect variance, the standard error for all tests can be calculated by taking the square root of this number.

STATISTICAL SIGNIFICANCE

In order to calculate the statistical significance of each variable, we will assume that the true effect of each variable is null. In other words, the Null and Alternative Hypotheses are

$$\begin{aligned} H_0 &: \mu_{effect} = 0 \\ H_a &: \mu_{effect} \neq 0 \end{aligned}. \tag{3}$$

Using this hypothesis test, the t-statistic for each estimate under the null hypothesis can be calculated with the expression

$$t = \frac{E_i - \mu_{effect}}{s_{effect}}. \tag{4}$$

For a t-distribution with 8 degrees of freedom, the 95% confidence interval for a two-tailed hypothesis test is t = 2.306. Therefore, any variables or interaction

variables with a t-statistic above this value can be assumed to have a significant effect on the final porosity of the sample.

Data Collection Procedure

The first step to determining the porosity of a sample was to create a sample that has no other intrinsic experimental value. In other words, this method requires a sample that can be destroyed without harming the rest of the research. In total, 16 samples were created (8 test conditions, replicated once) Once these samples were created, they were cleaned thoroughly. It is important to note that any cutting or grinding of an unaltered sample will cause damage to the delicate microstructures that exist at the substrate's surface. In order for this to be avoided, a solid medium needed to be placed in the voided regions of the dendritic structure. A low viscosity was used to fill in the vacant areas of the wicking structure. Several epoxies were considered, but Loctite 408 was determined to have the best combination of curing time, viscosity and odor. This was then allowed to dry overnight. It was very important to allow the epoxy to cure the full recommended time because when the sample is cut, the epoxy must be able to keep the copper dendrites from deforming under the stress of the blade.

Once the samples were prepared and encased in epoxy, the cut was made with a high-speed band saw. Then, the freshly cut faces were subjected to increasingly finer polishing techniques. First, heavy grit sandpaper was used to remove the teeth marks from the blade. Then, smaller grit sandpaper polished the sample further. Finally, very fine diamond sandpaper was used to polish the cut face to a shiny finish.

The sample was then put under a light microscope and series of pictures were taken. Since detail is very important to obtaining an accurate measure of porosity and pore radius, a 10x lens was used. Because this high magnification allows only a small view of the sample to be viewed, many pictures were taken and then assembled in MATLAB (See Appendix for code). In general, twenty six total pictures were needed per sample (more or less depending on the quality of the sample). An example of one of these pictures is given in Figure 4.

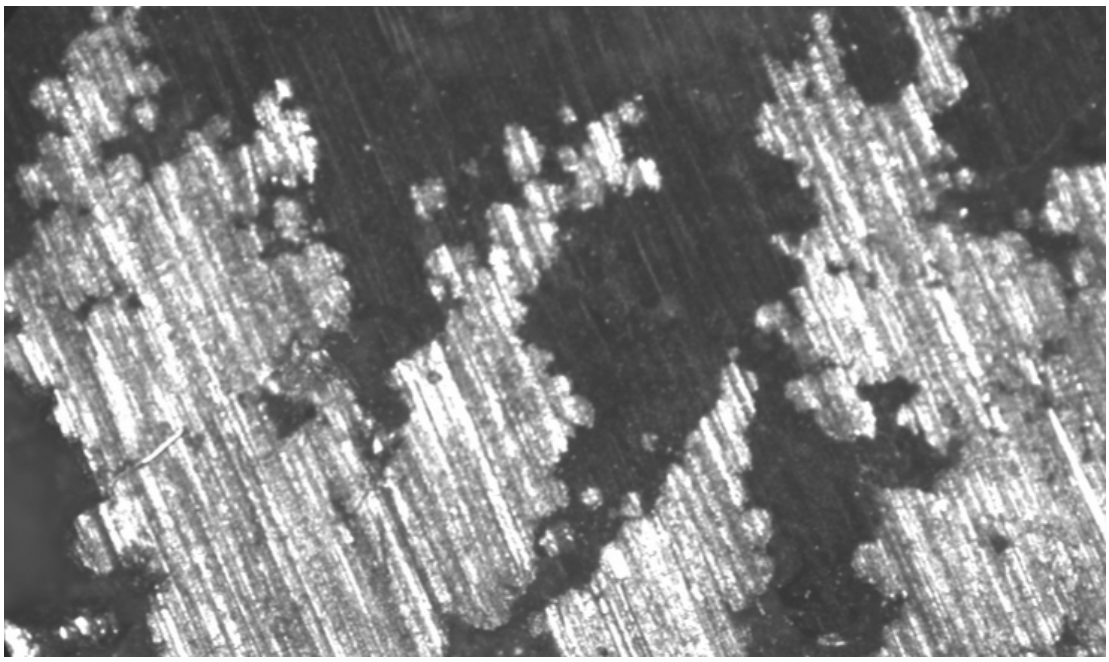

Figure 4. Sample image from the microscope imaging software

The next step was the process of assembling the individual pictures into a collaborative image. This process involved importing each microscope picture into MATLAB successively and manually choosing control points to match to two pictures. The MATLAB code in Appendix B [14] then takes these control points and rotates, translates, and scales the second figure and creates a collaborative image. An example of this can be seen in Figure 5.

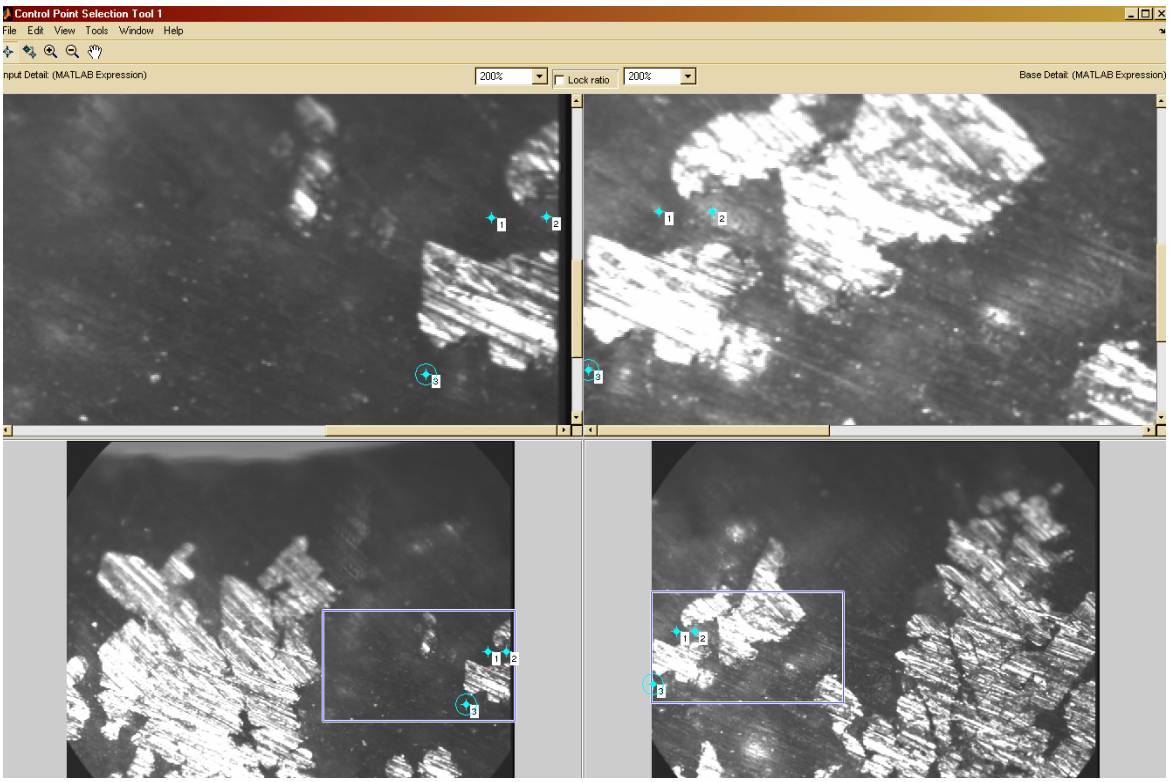

Figure 5. Control point selection for image consolidation in MATLAB.

Once this was done, the image was cropped so that the bottom edge of the picture was at the original substrate surface and the top edge of the picture was at the upper most edge of the wicking structure. Then, the image was imported into MATLAB and run through a brightness/contrast algorithm so that the copper portions of the picture had a brightness value of 255 (white) and the epoxy portions of the picture had a brightness value of 1 (black). The results of this algorithm can be seen in Figures 6 through 13. Then, the image was converted to a three dimensional matrix where each location in the matrix (corresponding to a particular pixel in the image) had a brightness value of either 255 or 1. This entire process was repeated to ensure that the first cut was a representative sample of the whole.

Chapter 4: Results

The results from the 2k factorial analysis were very good. In each of the experiment cases, the anode and cathode surface area ratios were held constant. Anode to cathode relationship is a very important part of electroplating and electroforming and plays an important role in the final product of wicks. Unfortunately, the sheer volume of variables this aspect of electroforming provides makes it a prohibitively massive parameter. Some of the many variables this aspect of the tests could include are: anode to cathode surface area, distance between anode and cathode, geometric similarities, edge effects and so on. A discussion on future suggestions for exploration will be discussed in the "Recommendations" section later. Also, all tests were run for 24 hours to allow the growths to "mature" for ease of analysis. Time is also an important factor in electroplating and electroforming. Unfortunately, time's effects are difficult to quantify due to its effect-overlap with current density, acidity, and salt concentration.

The final, high contrast images are given in Figures 8 through 13. These are shown to scale and the final porosity, height, and bath resistance are given in Table 3.

Samples

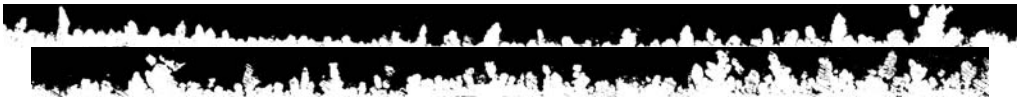

Figure 6. Final images for test condition 1.

Figure 7. Final images for test condition 2.

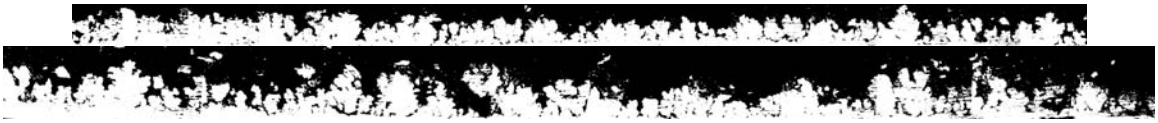

Figure 8. Final images for test condition 3.

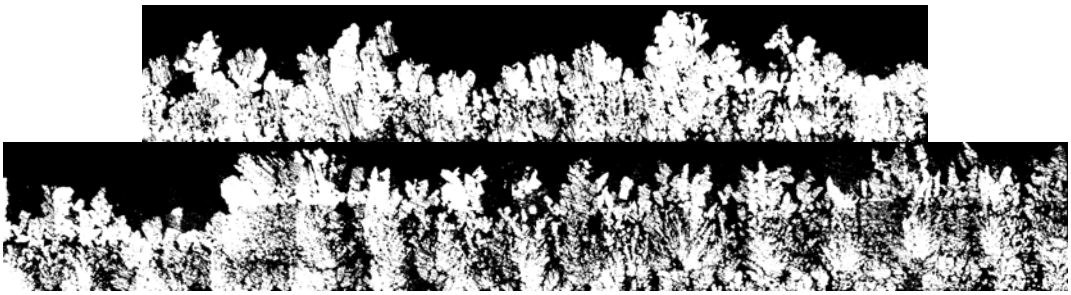

Figure 9. Final images for test condition 4.

Figure 10. Final images for test condition 5.

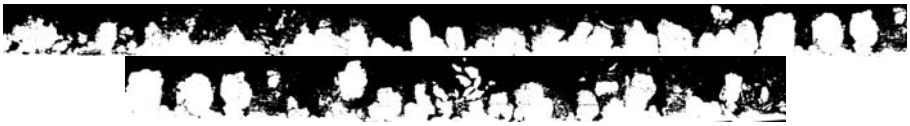

Figure 11. Final images for test condition 6.

Figure 12. Final images for test condition 7.

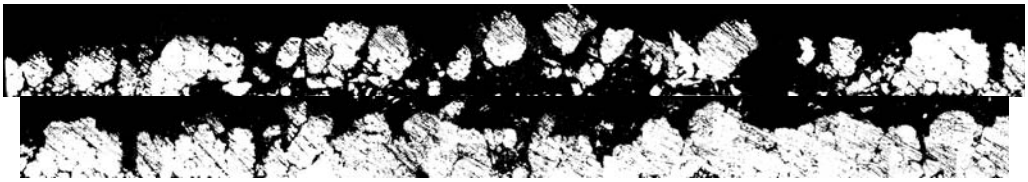

Figure 13. Final images for test condition 8.

Table 3. Results from the 2^k factorial experiment

	Porosity		Max wick height (mm)		Voltage	
	Run 1	Run 2	Run 1	Run 2	Run 1	Run 2
1	0.7053	0.6203	0.670412	0.7790262	3.75	3.7
2	0.7607	0.6467	0.8932584	1.0374532	14.6	14.71
3	0.4669	0.6127	0.6573034	0.7996255	1.1	0.98
4	0.52	0.541	2.1310861	2.2771536	3.6	3.29
5	0.4542	0.4957	0.258427	0.2322097	3.06	2.9
6	0.5226	0.5697	0.7677903	1.0168539	11	10.22
7	0.3492	0.3926	0.5093633	0.6479401	0.86	0.84
8	0.6876	0.4799	1.3483146	1.2134831	3.7	3.64

Result Analysis

Porosity is, as previously stated, an important parameter in determining the effectiveness of a wick. Porosity is used in the calculations for effective thermal conductivity, permeability, and pumping power. In fact, it is the most important variable when calculating effective thermal conductivity. It can be simply calculated by taking the ratio of voided regions to solid regions (MATLAB code in Appendix B). The factorial analysis calculations showed that the salt concentration and acidity of the electroforming bath play a statistically significant role in the final porosity of the sample as shown in Figure 14. Recall that statistically significant parameters are characterized as those with t-value greater than 2.306. The porosity profiles of these samples are given in Figures 17 and 28.

In addition, the “throwing power”, or the electroforming setup’s ability to build the wick faster is also an important factor although it is much less a function of acidity and salt content and more a function of the current density as shown in Figure 15.

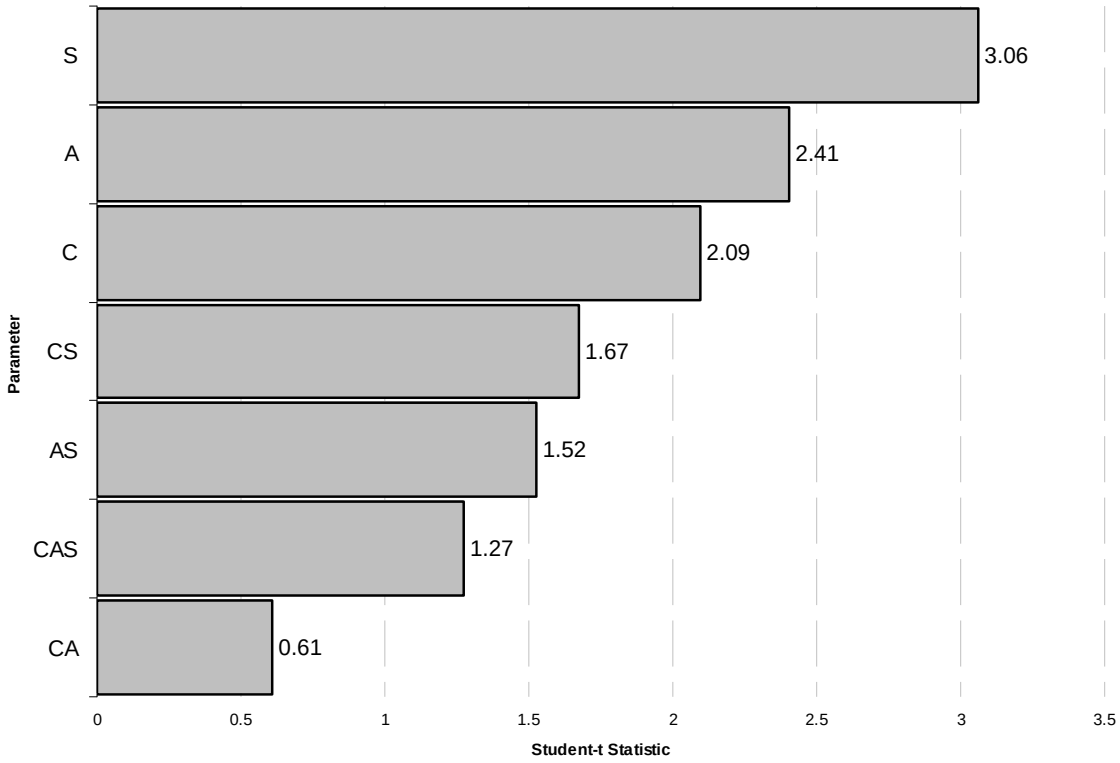

Figure 14. Pareto chart for effect on porosity of the wick

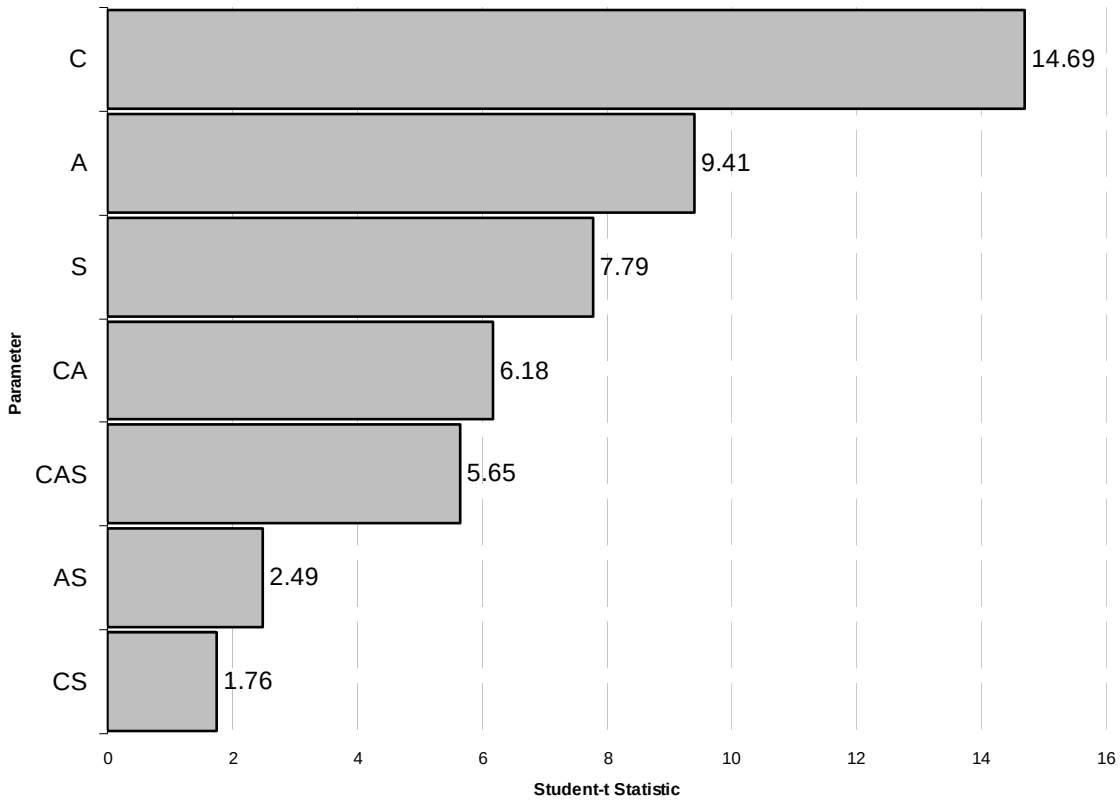

Figure 15. Pareto chart for effect on maximum wick height (throwing power).

Figure 16 describes the bath parameter effect on bath resistance. Also, it should be noted that the bath electrical resistance plays a large role in the final microstructure and macrostructure of the wick. In the case where the resistance of the bath is high (high voltage), the epitaxial growth (which is necessary for smooth plating) is nearly impossible. As discussed earlier, this condition occurs when atoms arrive at the substrate in large numbers. The “bunches” of crystallites arriving find areas on the substrate with the highest electrical potential and will discharge there. This leads to certain deposit orientations to grow preferentially.

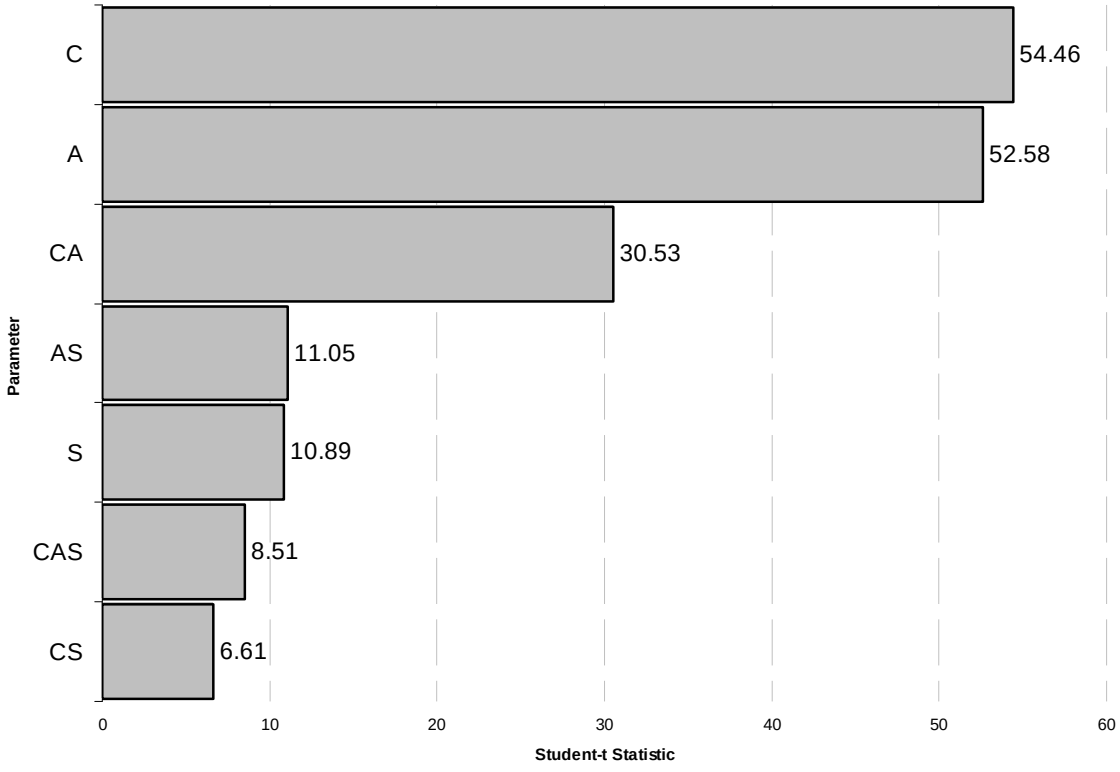

Figure 16. Pareto chart for effect on bath resistance (Voltage)

Porosity, due to its importance in determining the effectiveness of a wicking structure, was the first effect to be analyzed. Since effective thermal

conductivity and minimum capillary radius are inversely proportional to permeability, it is important to note that one value of porosity is not inherently better than another, but should be optimized based on the application. Figure 19 illustrates the porosity variation along the direction perpendicular to the substrate surface. As shown, the porosity wavers from the wall to the top layer of the wicks, which can significantly help the capillary performance and the effective thermal conductivity. In each image in Figure 17, there are two sets of data. These sets refer to the two repeated tests for each test sample. They were included to show the variation between two identical test conditions.

Test sample 1, shown in Figure 17(a), showed a very standard curve similar to the axial groove wick (Figure 4). The main difference is the non-linearity. This curve implies, and is confirmed by Figure 8, that the shape of the wick is porous at top and becomes more solid near the bottom.

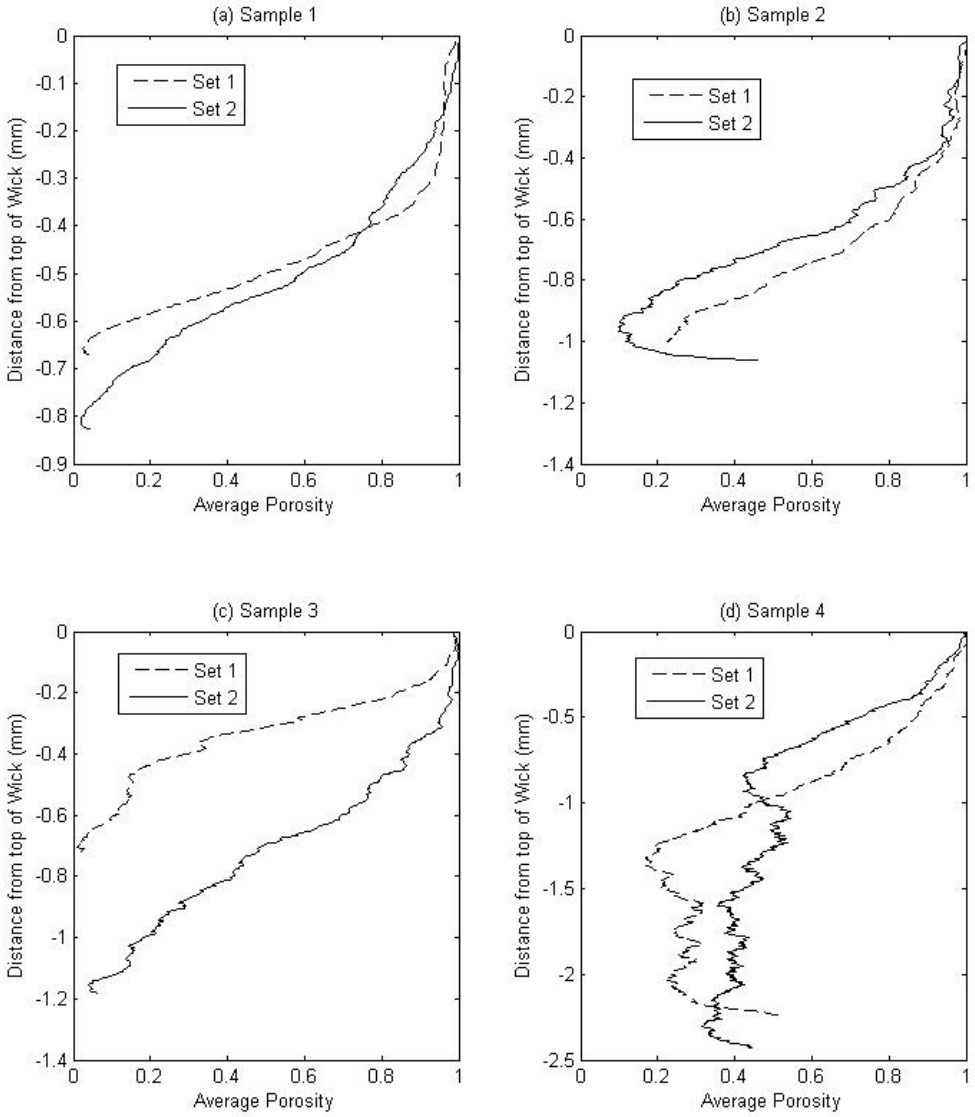
(a) Sample 1
Set 1
Set 2
Distance from top of Wick (mm)
Average Porosity
(b) Sample 2
Set 1
Set 2
Distance from top of Wick (mm)
Average Porosity
(c) Sample 3
Set 1
Set 2
Distance from top of Wick (mm)
Average Porosity
(d) Sample 4
Set 1
Set 2
Distance from top of Wick (mm)
Average Porosity

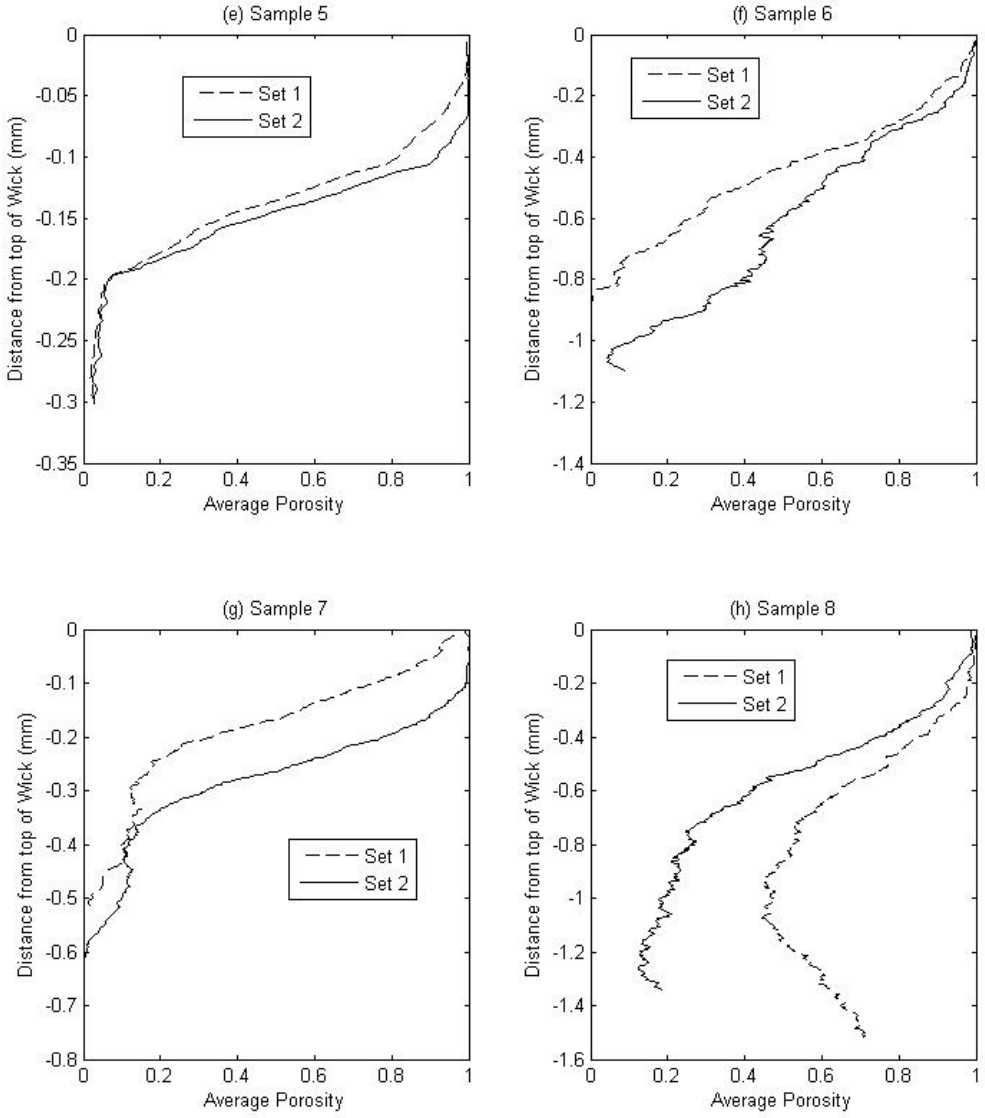

Figure 17. Vertical Porosity variation for test conditions 1 through 8

Test sample 2, shown in Figure 17(b), has a similar profile to sintered powder wicks (Figure 4). It is similar to Sample 1 in that it is more porous at the top, but decreases further down the wick. It is different from Sample 1 in that at some point from the top, the porosity actually increases. This is due to the nodular nature of the growth.

Test sample 3 shown in Figure 17(c) offers similar characteristics to Sample 1, but is taller and has a more pronounced drop in porosity. This implies that while porous and rough at the top of the wick, the structure fills out heavily near the bottom as shown in Figure 10.

Test sample 4, shown in Figure 17(d), is much different than all of the others thus far. Instead of becoming solid near the bottom of the wick, it levels off near a porosity of 0.4. By looking at Figure 11, it becomes clear that this is due to the massively dendritic nature of the structure.

The porosity profile in test sample 5, shown in Figure 17(e), suggests a smoother wick due to a very high porosity near the top of the wick (close to 1.0, or completely voided) and then a very sharp drop to a very low porosity (close to 0.0, or completely copper). It is also characterized by being considerably shorter than the other wicks.

The profile for test sample 6, shown in Figure 17(f), is very similar to Sample 2, but without the rebounded porosity near the base of the wick. This implies that the electrical potential was more evenly spaced on this sample than on test condition 2. The only difference between Samples 6 and 2 was the salt content, which indicates that the addition of copper ions from the salt led to a more even bond on the original substrate.

The profile for test sample 7, shown in Figure 17(g), has a similar shape to sample 5, but it is twice as tall. The only difference between the two tests was the acid content. This suggests that acid's ability to lower the bath resistance allowed for a more uninhibited growth. The high salt content in both test conditions 5 and

7 again supports the idea that the surplus of copper ions due to high salt content led to a stronger bond at the substrate surface.

Sample 8 shown in Figure 17(h) has a similar vertical porosity profile as Sample 2, but is more filled out at the bottom. If Set 1 on test condition 8 can be considered a deviation from the norm, the profile for this sample indicates that it fills out more effectively near the bottom of the wick than its low salt-counterpart in Sample 2.

PORE SIZE

Figures 18 through 25 illustrate the vertical variation on pore size. Pore size is a much more difficult parameter to characterize due to its wide variation even within exact test conditions. Because of this, a factorial analysis of pore size would yield unreliable results. Each test has to be examined individually to determine the acidity, salt, and current's effect on the vertical variation on pore size.

Pore size was analyzed with a MATLAB program (Appendix B) which scanned each image. For each row, the code looked for two pixels with a value of 255 (recall that this is the value for a white pixel, or one which suggests copper content) that were separated by a space with brightness values of 1 (voided pixels). The code then counted the number of pixels in this gap and, using the given image resolution, converted the distance to millimeters. This procedure yielded all of the pore sizes for a particular row of pixels. Then, after all pore sizes were measured for every row, the data was plotted against the height of the sample.

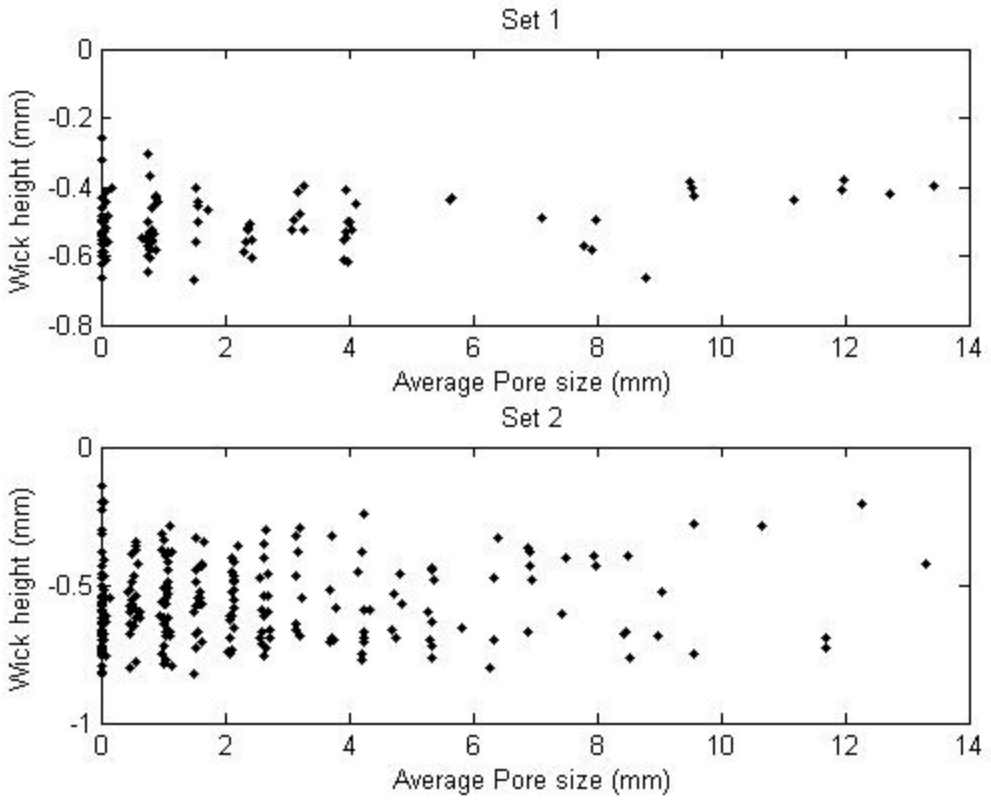

Figure 18. Vertical variation in pore size for test sample 1.

From test sample 1 (Figure 18), it can be seen that the pore size (in this case, pore diameter) varies from 0 to 14 mm with strong bunching between 0 and 4 mm. This case was characterized with low salt content, low acidity and low current density. As is the case will all test conditions, the analysis algorithm views image “noise” as pores. This can be seen with strong bunching of pores near the zero millimeter mark. These can be considered not applicable in the final analysis. Larger pore sizes, like those from 6mm+ are due to spikes in the wick and are not a strong indicator of the wick as a whole. These are not really “pores” but the distance between two high spikes in the wick.

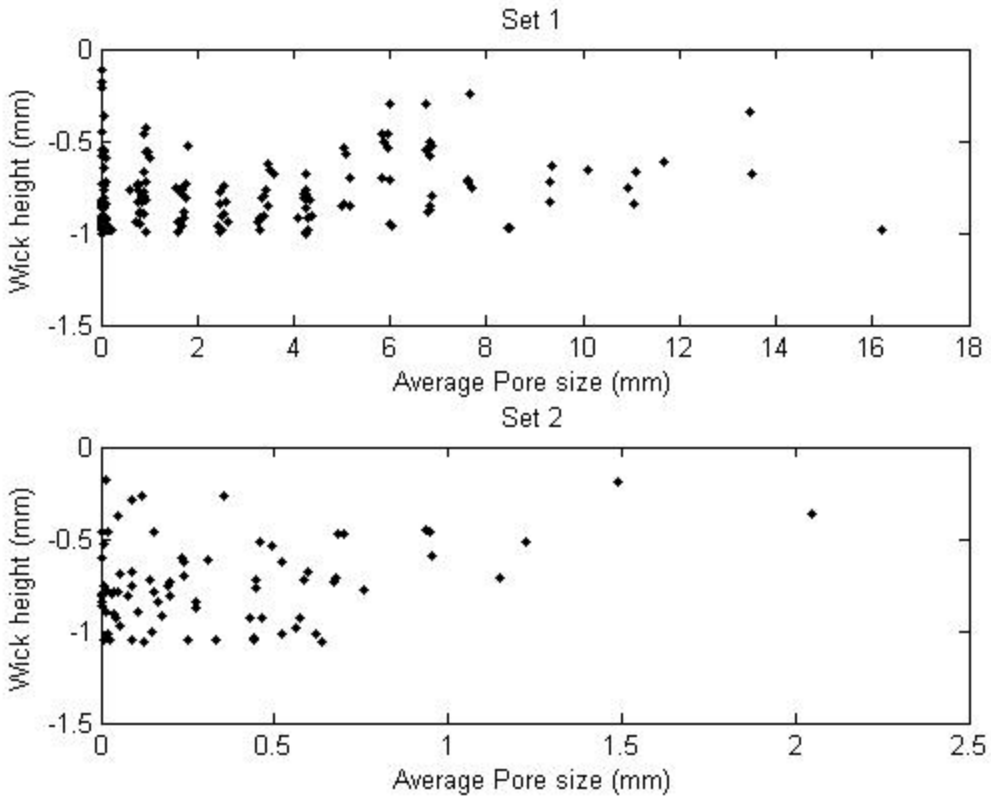

Figure 19. Vertical variation in pore size for test sample 2.

In test sample 2, it can be seen that there is a large bunching of pore sizes between 0 mm and 1 mm as seen in Figure 19. This test condition had low acidity and salt content, but high current density. Unfortunately, after testing, the wick in Set 2 was mishandled and dropped. This rendered a large portion of the wick useless for analysis. This is a case where limiting the total horizontal width of the analyzed sample removes large sections of pore size data. In Set 1, the total width of the sample was 15.6 mm and in Set 2, the total width of the sample was only 6.4 mm. However, if Set 1 is considered to representative of both cases, there is strong bunching of pore sizes between 0 and 6 mm. Once again, as was the case with test condition 1, the largest "pore" sizes are just distances between large spikes in the wick.

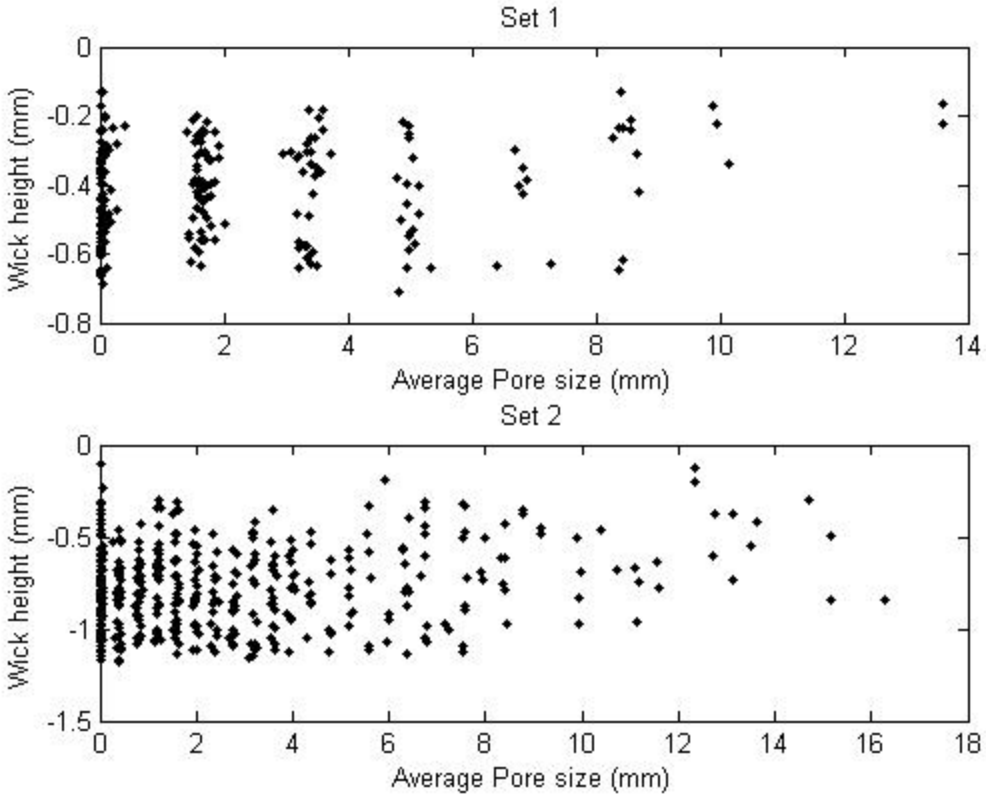

Figure 20. Vertical variation in pore size for test sample 3.

For test sample 3 (Figure 20), the pore bunching occurs between 0 and 6 mm but with much stronger bunching at pore sizes less than 4 mm. This test had high acidity, but low current and salt content.

For test sample 4 (Figure 21), the pore bunching occurs very heavily between 3 and 5 mm. This test condition had high current and acidity with low salt concentrations. Set 2 is considered to be a poor representative of the test condition due to the high volume of image noise. However, if Set 1 is considered representative of the test condition as a whole, two important points can be drawn from this data. First, there is a strong “treeing” effect in the wick which creates pores with diameters around 4 mm. Second, it is highly modal. The data in the 10+ mm range indicate that these trees are evenly spaced apart.

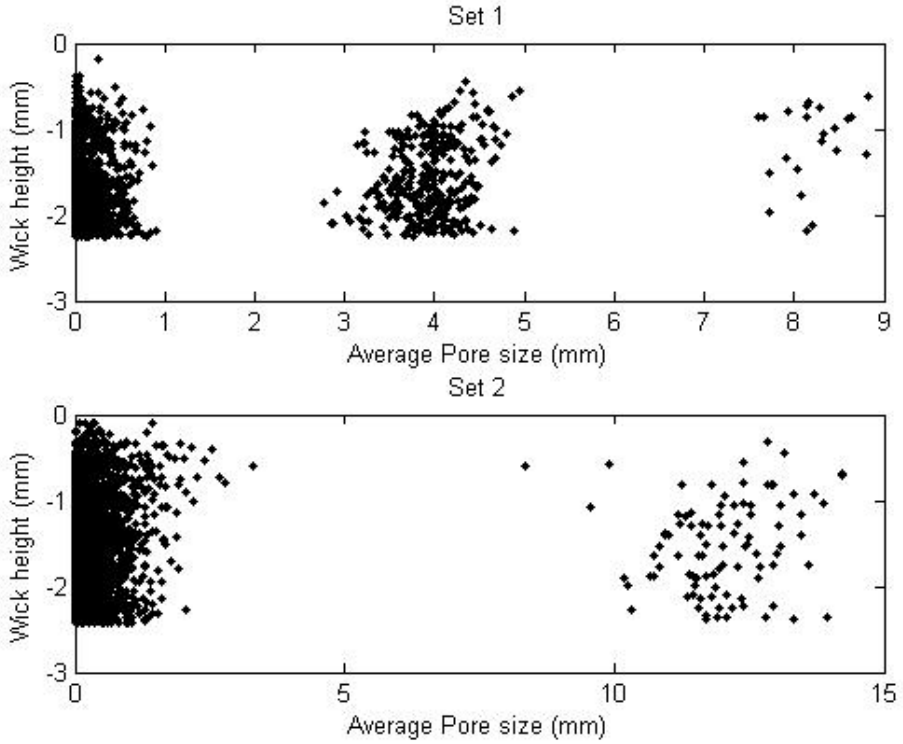

Figure 21. Vertical variation in pore size for test sample 4.

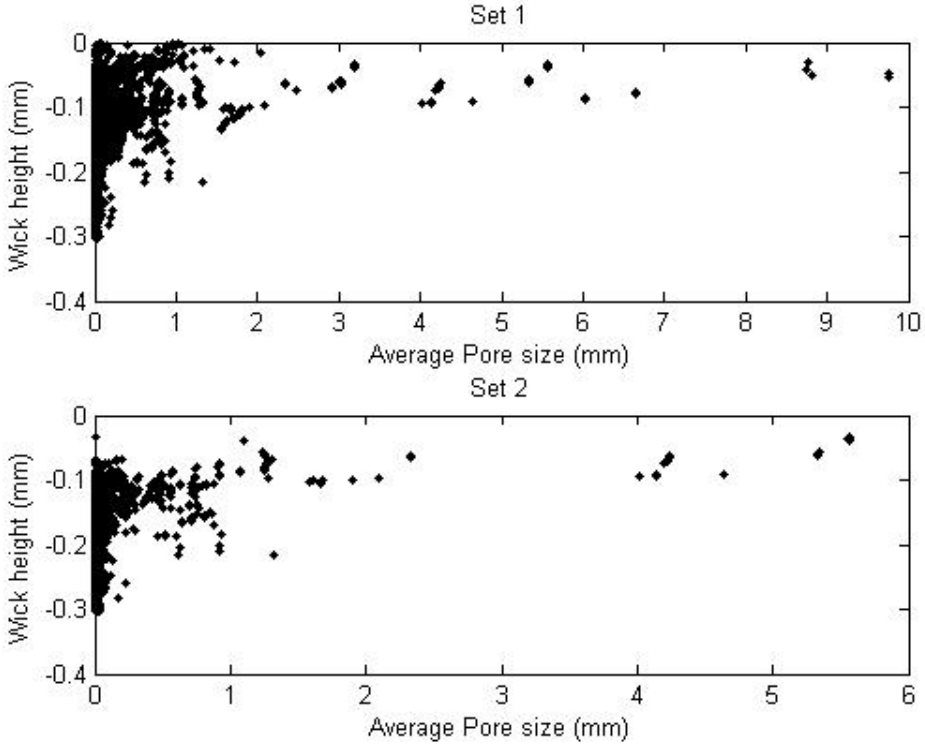

Figure 22. Vertical variation in pore size for test sample 5.

For test sample 5 (Figure 22), there is a strong bunching of points less than 1 mm. This test condition was characterized with low current density and acidity and high salt content. The very small pore size indicates (noise error aside) that the samples are relatively smooth. A look at Figure 12 shows that this, on a large scale, is true. However, the interesting part of these samples is the fact that, on a small scale, the sample has similar "treeing" effects as test samples 2 and 4.

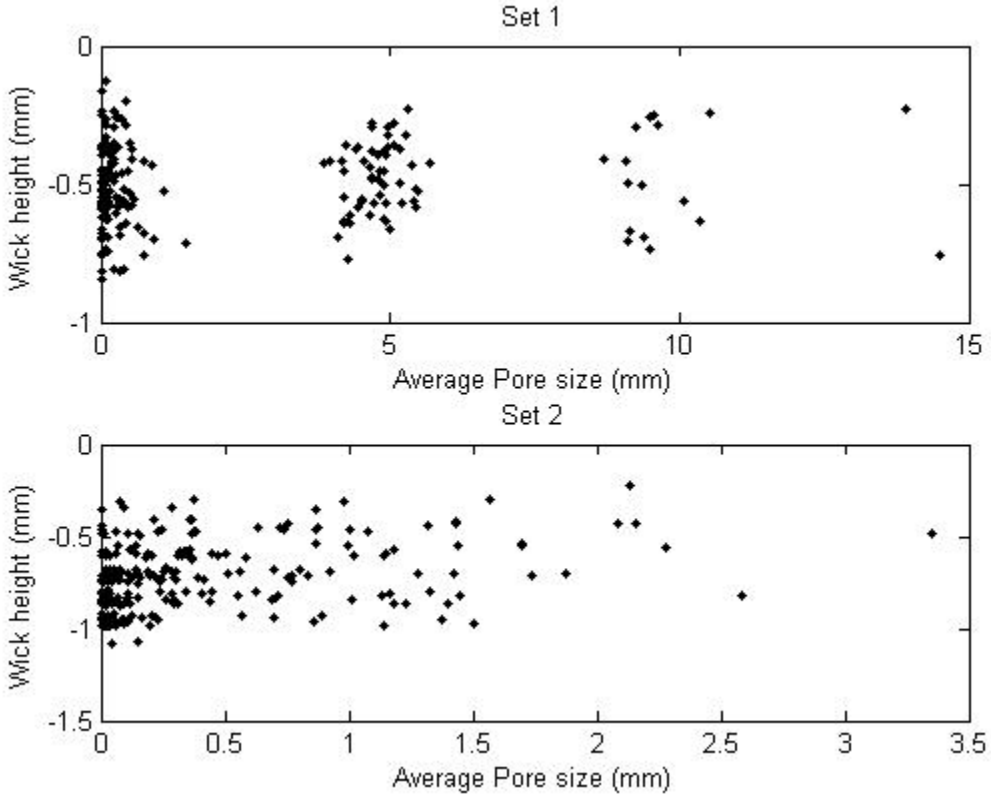

Figure 23. Vertical variation in pore size for test sample 6.

Test sample 6 (Figure 23) has strong bunching at pore sizes near 5 mm and less so at pore sizes near 10mm. This test was characterized with high current density and salt concentration with low acidity. Like test samples 2 and 4, the short horizontal length removes important data in Set 2. If Set 1 is considered to

representative of the test condition as a whole, this data suggests that, like test sample 4, the sample is modal. However, unlike test sample 4, this sample is more nodular, not dendritic as seen in Figure 11. This suggests that the low acid, high salt combination results in nodular growths, while the high acid, low salt combination results in dendritic growth.

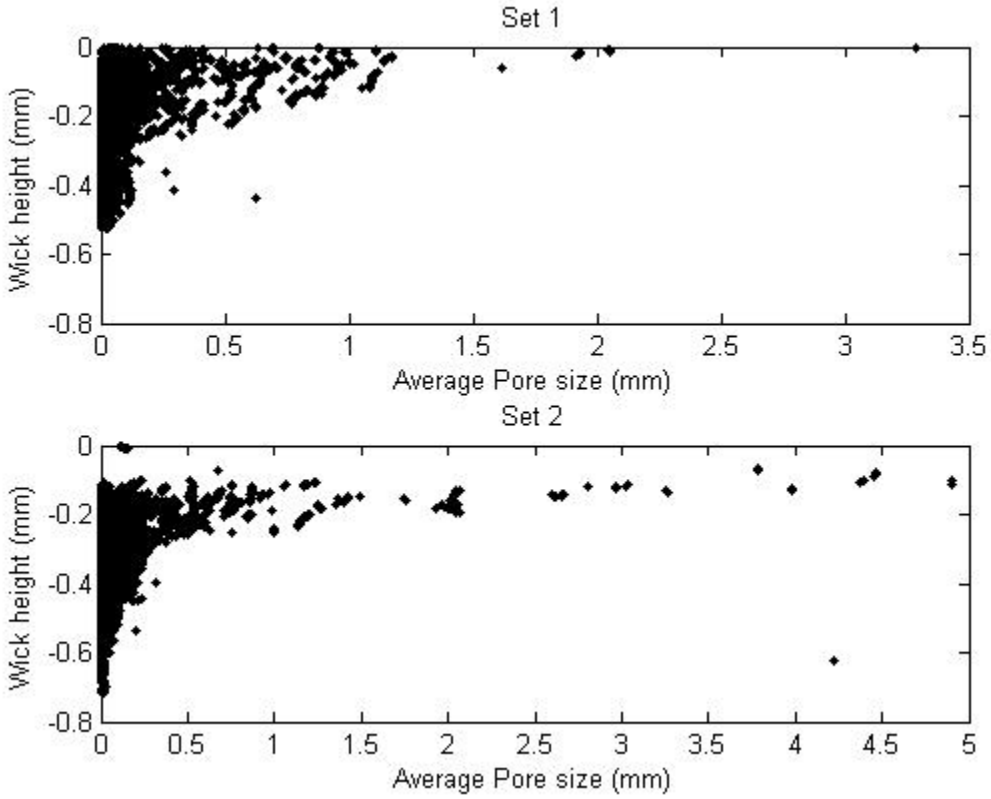

Figure 24. Vertical variation in pore size for test sample 7.

For test sample 7, there is no strong bunching at any pore size except near 0.5 mm. However, the data suggests that the majority of the pores are near the top of the sample and their sizes range between 0 and 5 mm. This test condition was characterized by a high salt and acid concentration, but with low current density. The data implies that this sample, more than the others before it, is thick

at the bottom of the sample, near the original substrate surface, and porous at the top.

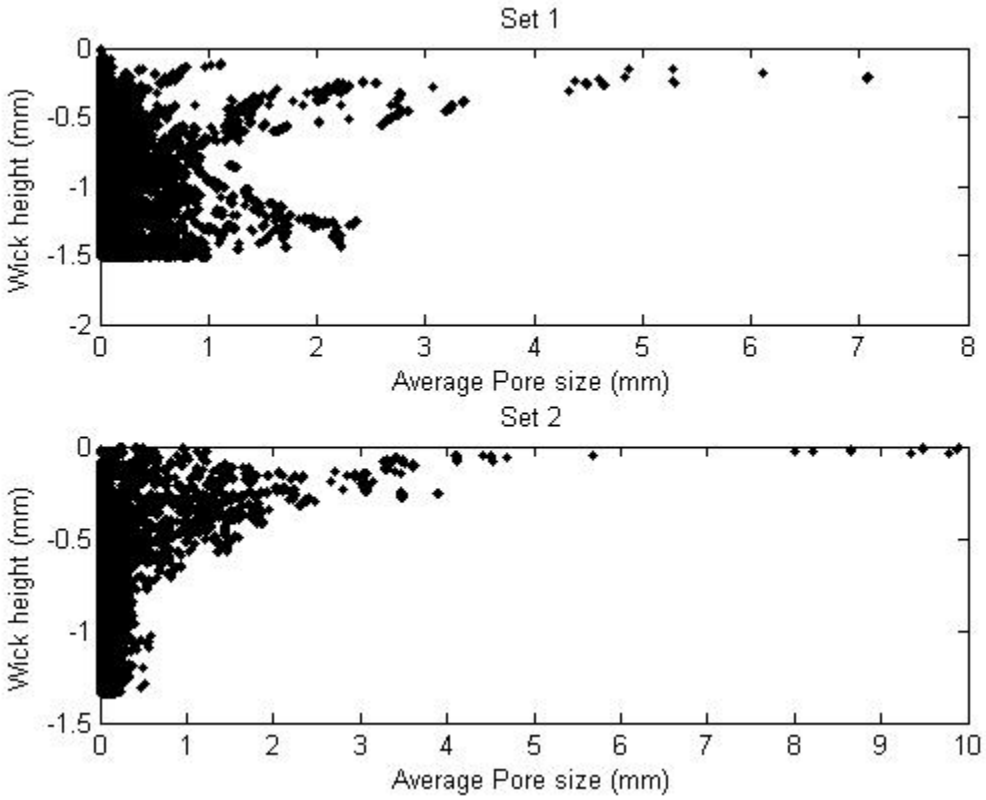

Figure 25. Vertical variation in pore size for test sample 8.

Test condition 8's data is very similar to test sample 7. This test was characterized by high values of current density, acidity and salt concentration. Like test sample 7, this data suggests that the majority of the pores are near the top of the wick, and it is less porous near the original substrate surface. Figure 12 also supports this data. The main difference between the two samples is the total height of the sample. Test sample 8, with its higher current density, resulted in a much higher wick.

Chapter 5: Conclusions

From the experimental results it can be concluded that this procedure can be used to create wicks with desired porosity, thermal conductivity, and pore radius, which can help to develop an optimized wick structure to be used in a highly efficient heat pipe. Early tests showed that low values of acid and salt yielded the most promising wicking structures. More specifically these values were acid content of less than 20 grams per liter of water and a salt content of less than 30 grams per liter of water. Current density was found to have a wider range of operation for creating suitable wicking structures with values ranging between 1.4 Amperes per decimeter (substrate surface area) and 5.2 Amperes per decimeter.

The results of the factorial analysis show that each of the three parameters tested (acid concentration, salt concentration, and current density) have a unique role in the final microstructure of an electroformed wick. The factorial analysis showed that the most statistically significant parameter in porosity was salt. It can be concluded that a high cupric sulfate content adds more copper ions to the electrolyte, allowing for larger “bunches” of electrodeposit crystallites to form away from the substrate. When these large “bunches” discharge at the surface of the cathode, it leads to a more nodular wick that closely resembles sintered powder wicks. In contrast, a lower salt content means that the “bunches” are smaller and more fiber-like. When these smaller “bunches” discharge at the surface of the cathode, it leads to a more dendritic wick. The acidity of the bath plays a more subtle, but no less important role in wick formation. A low acid

content raises the electrical resistance of the bath and creates paths of preferential electrical potential. This causes a columnar, modal growth which is characterized by areas of very high wick and equally low areas of wick height. A high acid content reduces these areas of high electrical potential and causes the wick to grow more uniformly. Current density (or amperage) is the parameter which governs “throwing power.” It has high interactivity with the other two, especially acidity. The combination of high acid, low salt and high current yields a very tall, columnar, dendritic structure. In contrast, the combination of high acid, low salt and low current yields a short, columnar, modal wick.

Each of these parameters could be individually tweaked to produce a wick which is suitable for the application at hand. The columnar, modal nature of low acid content and high salt content would be ideal for situations that would normally call on an axial groove wick. In a case where a high pumping power is required, the low salt and high acid combination creates a very porous medium with a very high surface area.

In conclusion, this procedure can be used to create any combination of thermal and fluid characteristics which could be needed in heat pipe cooling applications. It can be created quickly, economically, and at room temperature with comparable results to existing wicking structures.

RECCOMENDATIONS

To fully understand this process and the resulting wicking structure, much more research should be done. One aspect which was not covered here is the relationship between the anode and cathode. The problems which arise from not considering the surface area ratio between these two can be devastating. A high anode to cathode surface area will flood the electrolyte with copper ions and will result in occluded salts and poor bonding. A high cathode to anode surface area will starve the electrolyte of copper ions and will result in a stoppage of plating when the anode is consumed and will cause a safety hazard in the resulting open circuit. However, small variations in the surface area ratio can be beneficial. More research should be done to explore this aspect.

The fluid flow field is another aspect which was not covered, but may play an important role in the development of dendritic copper wicks. The interaction of how the fluid is moving past the substrate and the electrical field between anode and cathode is a large uncertainty in this application and it would be very interesting to explore this parameter. Similarly, the orientation of the cathode to anode in relation to one another is also of interest.

References

[1] Gaugler, R.S. Heat Transfer Device. *U.S. Patent 2350348,* 1942.

[2] Faghri, Amir. *Heat Pipe Science and Technology*. Taylor & Francis Group. 1995.

[3] Webb, R.L. and Kim, Nae-Hyun. *Principles of Enhanced Heat Transfer.* Taylor & Francis Group. 2005.

[4] Bejan, A. *Shape and Structure, from Engineering to Nature.* Cambridge University Press. 2000.

[5] Lowenheim, Frederick A. *Modern Electroplating, 3rd Edition.* Wiley-Interscience. 1974.

[6] Durney, Lawrence J. *Electroplating Engineering Handbook, Fourth Edition*. Von Nostrand Reinhold Company. 1984.

[7] Fujii, M., Nishiyama, E., and Yamanaka, G., Nucleate pool boiling heat transfer from microporous heating surface. *Advances in Enhanced Heat Transfer.* ASME, 1979.

[8] Shum, M.S., Finned Heat Transfer Tube with Porous Boiling Surface and Method for Producing Same. *U.S. Patent 4182412*. 1980.

[9] Vincent, Christopher. *Compact OHP and Development of Fuzzy Copper for Wicking Structures.* Masters thesis, University of Missouri-Columbia, 2008.

[10] Albertson, C., Nichols, G., and Rasmussen, J. Boiling Heat Transfer Surface, Method of Preparing Same and Method of Boiling. *U.S. Patent 4258783*. 1981.

[11] Grote, M., Stark, J., and Tefft, E. Enhanced Evaporator Surface. *U.S. Patent 4819719*. 1989.

[12] Masuda, Y., Takahashi, T., Takizawa, Y., Yoshiki, N., Heat Transfer Material. *U.S. Patent 4879185*. 1989.

[13] DeVor, Richard E. *Statistical Quality Design and Control.* Pearson Prentice Hall. 2007.

[14] Carroll, Michael and Davidson, Andrew. *Image Stitching with MATLAB.* 2007.

Table 4. Calculated Results of the Factorial Experiment for Porosity

	3	2	1	7	4	5	6	Rank			
	C	**A**	**S**	**CA**	**CS**	**AS**	**CAS**	**Run 1**	**Run 2**	**Avg**	**variance**
1	-	-	-	+	+	+	-	0.705	0.62	0.6628	0.003613
2	+	-	-	-	-	+	+	0.761	0.647	0.7037	0.006498
3	-	+	-	-	+	-	+	0.467	0.613	0.5398	0.010629
4	+	+	-	+	-	-	-	0.52	0.541	0.5305	0.000221
5	-	-	+	+	-	-	+	0.454	0.496	0.47495	0.000861
6	+	-	+	-	+	-	-	0.523	0.57	0.54615	0.001109
7	-	+	+	-	-	+	-	0.349	0.393	0.3709	0.000942
8	+	+	+	+	+	+	+	0.688	0.48	0.58375	0.02157
	-	-	-				-				
1	0.663	0.663	0.663	0.663	0.663	0.663	0.663			Pooled Variance:	0.00568
		-	-	-	-						
2	0.704	0.704	0.704	0.704	0.704	0.704	0.704			Effect Variance:	0.00142
3	-0.54	0.54	-0.54	-0.54	0.54	-0.54	0.54			Effect Standard Error:	0.037684
			-		-	-	-				
4	0.531	0.531	0.531	0.531	0.531	0.531	0.531				
	-	-			-	-					
5	0.475	0.475	0.475	0.475	0.475	0.475	0.475			Null Hypothesis: μ =	0
		-		-		-	-				
6	0.546	0.546	0.546	0.546	0.546	0.546	0.546			Significance Level: α =	0.025
	-			-	-		-				
7	0.371	0.371	0.371	0.371	0.371	0.371	0.371			For 95% CI: t >	2.306
8	0.584	0.584	0.584	0.584	0.584	0.584	0.584				
	0.079	0.091	0.115	0.023	0.063	0.057	0.048	**Main Effect**			
		-	-								
	0.079	0.091	0.115	0.023	0.063	0.057	0.048				
	C	**A**	**S**	**CA**	**CS**	**AS**	**CAS**				
	2.094	2.406	3.059	0.607	1.675	1.524	1.273	**t-statistic**			

Table 5. Calculated Results of the Factorial Experiment for wick height

	1	2	3	4	7	6	5	Rank			
	C	**A**	**S**	**CA**	**CS**	**AS**	**CAS**	**Run 1**	**Run 2**	**Avg**	**variance**
1	-	-	-	+	+	+	-	0.67	0.78	0.72	0.0059
2	+	-	-	-	-	+	+	0.893	1.04	0.97	0.0104
3	-	+	-	-	+	-	+	0.657	0.8	0.73	0.0101
4	+	+	-	+	-	-	-	2.131	2.28	2.2	0.0107
5	-	-	+	+	-	-	+	0.258	0.23	0.25	0.0003
6	+	-	+	-	+	-	-	0.768	1.02	0.89	0.031
7	-	+	+	-	-	+	-	0.509	0.65	0.58	0.0096
8	+	+	+	+	+	+	+	1.348	1.21	1.28	0.0091
	-	-	-				-				
1	0.725	0.725	0.725	0.725	0.725	0.725	0.725	Pooled Variance:			0.0109
		-	-	-	-						
2	0.965	0.965	0.965	0.965	0.965	0.965	0.965	Effect Variance:			0.0027
	-		-	-		-		Effect Standard			
3	0.728	0.728	0.728	0.728	0.728	0.728	0.728	Error:			0.0522
			-		-	-	-				
4	2.204	2.204	2.204	2.204	2.204	2.204	2.204				
	-	-			-	-					
5	0.245	0.245	0.245	0.245	0.245	0.245	0.245	Null Hypothesis: μ =			0
		-		-		-	-	Significance Level: α			
6	0.892	0.892	0.892	0.892	0.892	0.892	0.892	=			0.025
	-			-	-		-				
7	0.579	0.579	0.579	0.579	0.579	0.579	0.579	For 95% CI: t >			2.306
8	1.281	1.281	1.281	1.281	1.281	1.281	1.281				
	0.766	0.491	0.406	0.323	0.092	0.13	0.295	**Main Effect**			
			-		-		-				
	0.766	0.491	0.406	0.323	0.092	-0.13	0.295				
	C	**A**	**S**	**CA**	**CS**	**AS**	**CAS**				
	14.69	9.411	7.787	6.181	1.758	2.494	5.652	**t-statistic**			

Table 6. Calculated Results of the Factorial Experiment for Voltage

	1	2	5	3	7	4	6	**Rank**			
	C	**A**	**S**	**CA**	**CS**	**AS**	**CAS**	**Run 1**	**Run 2**	**Avg**	**variance**
1	-	-	-	+	+	+	-	3.75	3.7	3.725	0.00125
2	+	-	-	-	-	+	+	14.6	14.71	14.655	0.00605
3	-	+	-	-	+	-	+	1.1	0.98	1.04	0.0072
4	+	+	-	+	-	-	-	3.6	3.29	3.445	0.04805
5	-	-	+	+	-	-	+	3.06	2.9	2.98	0.0128
6	+	-	+	-	+	-	-	11	10.22	10.61	0.3042
7	-	+	+	-	-	+	-	0.86	0.84	0.85	0.0002
8	+	+	+	+	+	+	+	3.7	3.64	3.67	0.0018
	-	-	-				-				
1	3.725	3.725	3.725	3.725	3.725	3.725	3.725		Pooled Variance:		0.047694
		-	-	-	-						
2	14.66	14.66	14.66	14.66	14.66	14.66	14.66		Effect Variance:		0.011923
3	-1.04	1.04	-1.04	-1.04	1.04	-1.04	1.04		Effect Standard Error:		0.109194
			-		-	-	-				
4	3.445	3.445	3.445	3.445	3.445	3.445	3.445				
5	-2.98	-2.98	2.98	2.98	-2.98	-2.98	2.98		Null Hypothesis: μ =		0
		-		-		-	-		Significance Level: α		
6	10.61	10.61	10.61	10.61	10.61	10.61	10.61		=		0.025
7	-0.85	0.85	0.85	-0.85	-0.85	0.85	-0.85		For 95% CI: t >		2.306
8	3.67	3.67	3.67	3.67	3.67	3.67	3.67				
	5.946	5.741	1.189	3.334	0.721	1.206	0.929	**Main Effect**			
		-	-	-	-						
	5.946	5.741	1.189	3.334	0.721	1.206	0.929				
	C	**A**	**S**	**CA**	**CS**	**AS**	**CAS**				
	54.46	52.58	10.89	30.53	6.605	11.05	8.505	**t-statistic**			

Appendix B: MATLAB

imgcons.m

This file is used to assemble progressing microscope images into one collaborative image.

```
A={'output.jpg','1-2.bmp','1-3.bmp','1-4.bmp','1-5.bmp','1-6.bmp','1-
7.bmp','1-8.bmp','1-9.bmp','1-10.bmp','1-11.bmp','1-12.bmp','1-
13.bmp','1-14.bmp','1-15.bmp'};
N=15;

for i=2:N

    img1=imread(char(A(1)));
    img2=imread(char(A(i)));

    cpselect(rgb2gray(img1), rgb2gray(img2));
    pause;
    TFORM = cp2tform(input_points, base_points, 'linear conformal');
    [trans xdata ydata] = imtransform(img1, TFORM);
    [n o b] = size(trans);
    [l m z] = size(img2);

    if(xdata(1)<0)
        xdisp = -xdata(1) + 1;
        xdisp = round(xdisp);

        if(ydata(1)<0)
            ydisp = round(-ydata(1) + 1);
            imgsizex = max(n, l+ydisp-1);
            imgsizey = max(o, m+xdisp-1);

            canvas = uint8(zeros(imgsizex, imgsizey,3));
            canvas1 = uint8(zeros(imgsizex, imgsizey,3));
            canvas2 = uint8(zeros(imgsizex, imgsizey,3));

            canvas1(1:(n), 1:o, 1:z) = trans;
            canvas2(ydisp:(l+ydisp-1), xdisp:(m+xdisp-1), 1:z)= img2;

        else
            ydisp = round(1+ydata(1));
            imgsizex = max(n+ydisp-1, l);
            imgsizey = max(o, xdisp+m-1);

            canvas = uint8(zeros(imgsizex, imgsizey,3));
            canvas1 = uint8(zeros(imgsizex, imgsizey,3));
            canvas2 = uint8(zeros(imgsizex, imgsizey,3));

            canvas1(ydisp:(ydisp+n-1), 1:(o), 1:z) = trans;
            canvas2(1:(l), xdisp:(xdisp+m-1), 1:z)= img2;

        end
```

```
    else
        xdisp = xdata(1) + 1;
        xdisp = round(xdisp);

        if(ydata(1)<0)
            ydisp = round(-ydata(1) + 1);
            imgsizex = max(n, l+ydisp-1);
            imgsizey = max(o+xdisp-1, m);

            canvas = uint8(zeros(imgsizex, imgsizey,3));
            canvas1 = uint8(zeros(imgsizex, imgsizey,3));
            canvas2 = uint8(zeros(imgsizex, imgsizey,3));

            canvas1(1:(n), xdisp:(o+xdisp-1), 1:z) = trans;
            canvas2(ydisp:(ydisp+l-1), 1:(m), 1:z)= img2;

        else
            ydisp = round(1+ydata(1));
            imgsizex = max(n+ydisp-1, l);
            imgsizey = max(o+xdisp-1, m);

            canvas = uint8(zeros(imgsizex, imgsizey,3));
            canvas1 = uint8(zeros(imgsizex, imgsizey,3));
            canvas2 = uint8(zeros(imgsizex, imgsizey,3));

            canvas1(ydisp:(n+ydisp-1), xdisp:(xdisp+o-1), 1:z) = trans;
            canvas2(1:(l), 1:(m), 1:z)= img2;

        end
    end
    canvassub = imsubtract(canvas1, canvas2);
    canvas = imadd(canvassub,canvas2);

    imwrite(canvas, 'output.jpg');

    imshow(canvas);
    pause;

    clc
    clear input_points base_points
    close all

end
```

porosity.m

This file is used to take an existing high contrast assembled wick image and calculate porosity of the sample.

```
function [G,M,D]=porosity(R)
T=imread(R); %converts image to matrix
Y=mean(T); %finds average of each column
Q=size(T);
cc=.0018726592;  %pixel to mm conversion
```

```
for i=1:Q(1)
    D(i)=i*cc;
    U(i)=mean(T(i,:)); %finds average of each row
end
M=1-U/255;
figure
plot(M,-D,'k')
xlabel('Average Porosity')
ylabel('Distance from top of Wick (mm)')
axis([0 1 min(-D) max(-D)])
X=cc*[1:1:length(Y)]; %sets up sample length
A=mean(Y); %finds copper amount (out of 255)
G=1-A/255; %porosity
H=G*ones(1,length(Y));%porosity line
figure
plot(X,1-Y/255,'k',X,H,'k:')
xlabel('Length along sample (mm)')
ylabel('Porosity')
axis([min(X) max(X) min(1-Y/255) max(1-Y/255)])
```

pordata2.m

This file is used to take the m-file porosity.m and display images and data for each sample relating to porosity.

```
[G,M1,D1]=porosity('1-1.jpg');
[G,M2,D2]=porosity('1-2.jpg');
[G,M3,D3]=porosity('2-1.jpg');
[G,M4,D4]=porosity('2-2.jpg');
[G,M5,D5]=porosity('3-1.jpg');
[G,M6,D6]=porosity('3-2.jpg');
[G,M7,D7]=porosity('4-1.jpg');
[G,M8,D8]=porosity('4-2.jpg');
[G,M9,D9]=porosity('5-1.jpg');
[G,M10,D10]=porosity('5-2.jpg');
[G,M11,D11]=porosity('6-1.jpg');
[G,M12,D12]=porosity('6-2.jpg');
[G,M13,D13]=porosity('7-1.jpg');
[G,M14,D14]=porosity('7-2.jpg');
[G,M15,D15]=porosity('8-1.jpg');
[G,M16,D16]=porosity('8-2.jpg');
[G,M17,D17]=porosity('sinteredpowder.jpg');
[G,M18,D18]=porosity('axialgroove(tri).jpg');

figure
subplot(2,2,1), plot(M1,-D1,'k--',M2,-D2,'k')
title('Sample 1')
xlabel('Average Porosity')
ylabel('Distance from top of Wick (mm)')
legend('Set 1','Set 2')

subplot(2,2,2), plot(M3,-D3,'k--',M4,-D4,'k')
title('Sample 2')
xlabel('Average Porosity')
ylabel('Distance from top of Wick (mm)')
legend('Set 1','Set 2')
```

```
subplot(2,2,3), plot(M5,-D5,'k--',M6,-D6,'k')
title('Sample 3')
xlabel('Average Porosity')
ylabel('Distance from top of Wick (mm)')
legend('Set 1','Set 2')

subplot(2,2,4), plot(M7,-D7,'k--',M8,-D8,'k')
title('Sample 4')
xlabel('Average Porosity')
ylabel('Distance from top of Wick (mm)')
legend('Set 1','Set 2')

figure
subplot(2,2,1), plot(M9,-D9,'k--',M10,-D10,'k')
title('Sample 5')
xlabel('Average Porosity')
ylabel('Distance from top of Wick (mm)')
legend('Set 1','Set 2')

subplot(2,2,2), plot(M11,-D11,'k--',M12,-D12,'k')
title('Sample 6')
xlabel('Average Porosity')
ylabel('Distance from top of Wick (mm)')
legend('Set 1','Set 2')

subplot(2,2,3), plot(M13,-D13,'k--',M14,-D14,'k')
title('Sample 7')
xlabel('Average Porosity')
ylabel('Distance from top of Wick (mm)')
legend('Set 1','Set 2')

subplot(2,2,4), plot(M15,-D15,'k--',M16,-D16,'k')
title('Sample 8')
xlabel('Average Porosity')
ylabel('Distance from top of Wick (mm)')
legend('Set 1','Set 2')

figure
subplot(2,1,1), plot(M17,-D17,'k')
title('Sintered Metal Powders')
xlabel('Average Porosity')
ylabel('Distance from top of Wick (mm)')

subplot(2,1,2), plot(M18,-D18,'k')
title('Triangular Axial Grooves')
xlabel('Average Porosity')
ylabel('Distance from top of Wick (mm)')
```

reff.m

This file is used to take an existing high contrast assembled wick image and calculate various pore radius data.

```
function [stats,dx2,re]=reff(R)
```

```
I=imread(R); %converts image to matrix
S=size(I);
cc=.0018726592;
st=0;
en=0;
k=1;
for i=1:S(1)
    for j=1:(S(2)-1)
        if I(i,j)==255 && I(i,j+1)==0
            st=j;
        elseif I(i,j)==0 && I(i,j+1)==255 && st~=0
            en=j;
        end
        if st*en~=0
            dx(k,1)=en-st;
            dx(k,2)=i;
            k=k+1;
            st=0;
            en=0;
        end
    end
    st=0;
    en=0;
end
u=1;
for n=1:S(1)
    if isempty(dx(dx(:,2)==n))==0
        t=dx(dx(:,2)==n);
        avgt(u)=mean(t(:,1));
        sdt(u)=std(t(:,1));
        mint(u)=min(t(:,1));
        maxt(u)=max(t(:,1));
        nt(u)=n;
        u=u+1;
    end
end
stats=cc*[nt',avgt',sdt',mint',maxt'];
dx2=cc*dx;
re=cc*mean(avgt');
```

pordata.m

This file is used to take the m-file reff.m and display images and data for each sample relating to pore size.

```
[stats, dx1, re]=reff('1-1.jpg');
[stats, dx2, re]=reff('1-2.jpg');
figure
subplot(2,1,1),plot(dx1(:,1),-dx1(:,2),'k.')
xlabel('Average Pore size (mm)')
ylabel('Wick height (mm)')
title('Set 1')
subplot(2,1,2),plot(dx2(:,1),-dx2(:,2),'k.')
xlabel('Average Pore size (mm)')
ylabel('Wick height (mm)')
title('Set 2')
```

```
[stats, dx3, re]=reff('2-1.jpg');
[stats, dx4, re]=reff('2-2.jpg');
figure
subplot(2,1,1),plot(dx3(:,1),-dx3(:,2),'k.')
xlabel('Average Pore size (mm)')
ylabel('Wick height (mm)')
title('Set 1')
subplot(2,1,2),plot(dx4(:,1),-dx4(:,2),'k.')
xlabel('Average Pore size (mm)')
ylabel('Wick height (mm)')
title('Set 2')

[stats, dx5, re]=reff('3-1.jpg');
[stats, dx6, re]=reff('3-2.jpg');
figure
subplot(2,1,1),plot(dx5(:,1),-dx5(:,2),'k.')
xlabel('Average Pore size (mm)')
ylabel('Wick height (mm)')
title('Set 1')
subplot(2,1,2),plot(dx6(:,1),-dx6(:,2),'k.')
xlabel('Average Pore size (mm)')
ylabel('Wick height (mm)')
title('Set 2')

[stats, dx7, re]=reff('4-1.jpg');
[stats, dx8, re]=reff('4-2.jpg');
figure
subplot(2,1,1),plot(dx7(:,1),-dx7(:,2),'k.')
xlabel('Average Pore size (mm)')
ylabel('Wick height (mm)')
title('Set 1')
subplot(2,1,2),plot(dx8(:,1),-dx8(:,2),'k.')
xlabel('Average Pore size (mm)')
ylabel('Wick height (mm)')
title('Set 2')

[stats, dx9, re]=reff('5-1.jpg');
[stats, dx10, re]=reff('5-2.jpg');
figure
subplot(2,1,1),plot(dx9(:,1),-dx9(:,2),'k.')
xlabel('Average Pore size (mm)')
ylabel('Wick height (mm)')
title('Set 1')
subplot(2,1,2),plot(dx10(:,1),-dx10(:,2),'k.')
xlabel('Average Pore size (mm)')
ylabel('Wick height (mm)')
title('Set 2')

[stats, dx11, re]=reff('6-1.jpg');
[stats, dx12, re]=reff('6-2.jpg');
figure
subplot(2,1,1),plot(dx11(:,1),-dx11(:,2),'k.')
xlabel('Average Pore size (mm)')
ylabel('Wick height (mm)')
title('Set 1')
```

```
subplot(2,1,2),plot(dx12(:,1),-dx12(:,2),'k.')
xlabel('Average Pore size (mm)')
ylabel('Wick height (mm)')
title('Set 2')

[stats, dx13, re]=reff('7-1.jpg');
[stats, dx14, re]=reff('7-2.jpg');
figure
subplot(2,1,1),plot(dx13(:,1),-dx13(:,2),'k.')
xlabel('Average Pore size (mm)')
ylabel('Wick height (mm)')
title('Set 1')
subplot(2,1,2),plot(dx14(:,1),-dx14(:,2),'k.')
xlabel('Average Pore size (mm)')
ylabel('Wick height (mm)')
title('Set 2')

[stats, dx15, re]=reff('8-1.jpg');
[stats, dx16, re]=reff('8-2.jpg');
figure
subplot(2,1,1),plot(dx15(:,1),-dx15(:,2),'k.')
xlabel('Average Pore size (mm)')
ylabel('Wick height (mm)')
title('Set 1')
subplot(2,1,2),plot(dx16(:,1),-dx16(:,2),'k.')
xlabel('Average Pore size (mm)')
ylabel('Wick height (mm)')
title('Set 2')
```